Maternal–fetal inflammation affects *Cdh1*/E-cadherin epigenetic regulation and craniofacial development

Diogo Nani[1,2], Lucas Alvizi[3], Heloisa Maria de Siqueira Bueno[2], Ellen Cristina Miranda Lacerda[1], Chao Yun Irene Yan[4], and Maria Rita Passos-Bueno[1,2*]

[1] Department of Genetics and Evolutionary Biology, Institute of Biosciences, University of São Paulo. São Paulo, Brazil.

[2] Human Genome and Stem Cell Research Center, University of São Paulo. São Paulo, Brazil.

[3] Department of Cell and Developmental Biology, University College London. London, UK.

[4] Department of Cell and Developmental Biology, Institute of Biomedical Sciences, University of São Paulo. São Paulo, Brazil.

*Corresponding author: MR Passos-Bueno (passos@ib.usp.br).

Key words: *CDH1*, E-cadherin, neural crest, gene-environment, epigenetics, immune activation, mouse, cleft lip and palate

Abstract

Cleft lip with or without palate (CLP) is a multifactorial trait associated with environmental exposures such as smoking, alcohol consumption, and pro-inflammatory conditions during early pregnancy, as well as with both common and rare genetic variants. Our group identified *CDH1* loss-of-function variants segregating in families with CLP, with incomplete penetrance linked to promoter hypermethylation. Previously, we demonstrated that gene-environment interactions driven by pro-inflammatory factors can induce this methylation, downregulate E-cadherin expression, and impair neural crest migration, thereby contributing to the etiology of CLP. However, the embryonic consequences of the two-hit CLP model (*CDH1* haploinsufficiency combined with pro-inflammatory insult) have not yet been explored in mammals. Here, under single dose of floxed-*Cdh1*, we investigated the pro-inflammatory response at the maternal-fetal interface, its impact on cytokine and *Cdh1* expression along the anteroposterior axis, the associated epigenetic landscape in the embryonic head, and the effect on cranial structures. We found that pro-inflammatory activation differentially signals to the embryo between anterior and posterior regions, impairing *Cdh1*/E-cadherin expression in NC cells of the head, accompanied by *Cdh1* promoter hypermethylation and other differentially methylated genes involved in cell-junction maintenance. Our findings support a model in which maternal pro-inflammatory responses act as environmental factors that repress NC *CDH1* expression through epigenetic mechanisms, contributing to CLP

development by downregulating E-cadherin and potentially compromising overall epithelial integrity. Animal Ethics Committee (CEUA IB/USP) number approval: 394/2022

Introduction

Cleft lip with or without cleft palate (CLP) is a multifactorial trait considered to be the most prevalent craniofacial malformation worldwide, affecting in average 1:1,000 live-births(1–4), with significant financial and psychosocial impacts(5–8). Aside from suffering impairments in breathing and sleeping(9), swallowing(10) and vocalization(11), CLP represents a significant cost to health systems. A Canadian study observed patients from 1999 to 2021, and estimated the average cost for CLP care at U$73.398,00(12). Also, a study from the Netherlands has estimated the average cost for treatment, between 0 and 24 years of age, as €40.859,00(8). In the state of Paraná, Brazil, it was estimated that treatment complementary to reconstruction surgeries is R$ 18.992,98 (13).

Common and rare genetic variants in genes of cell surface adhesion and mobility molecules, growth and transcription factors, nutrient metabolism enzymes and immune system components have been associated with CLP(14,15). Single nucleotide polymorphisms (SNPs) in genes of morphogens and transcription factors, such as *WNT3*, *WNT9B*, *WNT10A*, *AXIN2* e *MSX1*, are associated with predisposition to CLP with small impact, but significant cumulative effects(16–18). On the other hand, harbouring a single rare variant that affects central genes in the canonic Wnt/β-catenin pathway, such as *CTNNB1*, *AXIN2*, *GSK3B* and *LRP6* confer high risk for CLP(16). Modifications in the proliferation and migration of neural crest (NC), caused by alterations in the cellular cadherin complex, such as the ones related to Epithelial-to-Mesenchymal Transition (EMT), are related to the etiology of craniofacial abnormalities(14,19–25). Some studies have pointed to the role of *CDH1* variants in CLP(23,26,27). *CDH1* encodes for the epithelial cadherin (E-cadherin), which plays an important role in cell adhesion and signalling involved in morphogenesis processes(26–33). Responsible for adherens junctions in cell-cell contact, E-cadherins are key structural factors for epithelial integrity so that null *CDH1* mutant embryos are unviable due to failure in trophectoderm development(34,35). E-cadherin also plays an important signaling role in combination with β-catenin (*CTNNB1*) and p120ctn (*CTNND1*) in the Wnt pathway(36). Disturbances in this function can directly affect migration, polarization and organization of cells during craniofacial development. Evidence in mouse models have shown that alterations in the Wnt/β-catenin pathway, including deletions in *Cdh1*, *Ctnnb1* and *Ctnnd1* result in facial and tooth malformation(36–38). Specifically on NC ontogeny, the EMT-associated E-cadherin to N-cadherin (*CDH2*) switch plays an important role in delamination prior to the migration and differentiation of craniofacial structures(27,39)

. Therefore, disturbances in NC *CDH1* regulation are thought to affect craniofacial development(4,40,41).

E-cadherin is also known as a tumour suppressor(42) . Mutations in *CDH1* are central to the pathogenesis of Diffuse Gastric and Lobular Breast Cancer Syndrome (DGLBC) (OMIM #137215), an inherited condition that accounts for 1-3% of stomach cancers, which can occur with or without CLP(42,43). *CDH1* pathogenic variants are also linked to autosomal dominant blepharocheilodontic syndrome 1 (OMIM # 119580) (44,45). Loss of E-cadherin drives cells to mesenchymal phenotype, disrupting tissue architecture and promoting invasiveness, a hallmark of DGLBC(43). It also plays a role in other epithelial-derived cancers, such as in oral squamous cell carcinoma, in which E-cadherin expression, as well as podoplanin and vimentin, have been evaluated as a marker of EMT(46). In DGLBC, tumorigenesis typically follows the two-hit hypothesis, wherein a germline *CDH1* pathogenic variant is followed by a second somatic event, such as promoter hypermethylation, loss of heterozygosity, allele-specific silencing, or somatic mutation, leading to E-cadherin inactivation and malignant transformation(46–49). DNA methylation is not limited to cancer progression. It also plays a vital role in developmental disorders. *CDH1* genetic variants(50), and promoter hypermethylation, has been identified in non-syndromic CLP, the latter suggesting a potential epigenetic second hit that contributes to disease penetrance in individuals already carrying germline *CDH1* mutations(49,51).

The “two-hit” hypothesis is a genetic model that explains how certain diseases may arise not from a single genetic mutation, but from the combined effects of two distinct genetic or environmental insults. The first “hit” typically involves an inherited germline mutation that alone may not result in disease but establishes a predisposed state. The second “hit” is usually a somatic mutation or environmental factor occurring later in development, triggering disease manifestation. For instance, the recurrent 16p12.1 microdeletion has been identified as a risk factor for neurodevelopmental disorders, and many individuals carrying this deletion remain asymptomatic unless a second large copy number variation is also present, supporting the two-hit model(52,53). Similarly, in schizophrenia, early disruptions in cell signaling pathways during central nervous system development (first hit) may predispose individuals to later dysfunction when these same pathways are reactivated or stressed during adolescence (second hit)(54). Animal models further support this. Mice with a heterozygous deletion in *Cntnap2* exhibit neurobehavioral impairments only when exposed to early-life stressors, revealing how gene-environment interactions can converge to produce a complex phenotype(55). In hereditary hemorrhagic telangiectasia, vascular malformations, including craniofacial arteriovenous malformations, have been shown to require biallelic inactivation of disease-related genes like *SMAD4*, consistent with a two-hit mechanism involving both inherited and somatic mutations(56). Craniofacial disorders such as

craniofacial microsomia further illustrate this. Pathogenic variants in *FOXI3* were often inherited from unaffected parents, suggesting that additional genetic modifiers or environmental exposures may be required to fully express the phenotype(57). The interplay between genetic mutations and environmental insults, such as ethanol, also exemplifies a two-hit scenario. Ethanol-induced craniofacial defects in *Bmp* mutant zebrafish were attributed to increased apoptosis in cranial NC, which are essential for craniofacial morphogenesis(58). These findings underscore the importance of NC survival and signaling interactions with surrounding tissues, which are vulnerable to disruption by concurrent genetic mutations and environmental insults, ultimately driving the spectrum of craniofacial anomalies. Therefore, gene-environmental interactions involved in cell migration and differentiation affect craniofacial cartilage and bone development(15,59–61).

Such gene-environmental interactions such as intrauterine exposure to maternal cytokines, transferred via placental circulation, can induce fetal development modifications of clinical relevance(62–64). Pro-inflammatory activation has been related to impairments involved in orofacial clefts(65–70) with entangled epigenetic regulation(71), and studies have pointed to *CDH1* hypermethylation/E-cadherin downregulation owing to immune activation(72–77). Our group has previously identified heterozygous *CDH1* loss of function variants segregating in families of CLP patients, and associated with incomplete penetrance, estimated as ~50%(78). It was further demonstrated that CLP penetrance in *CDH1*$^{+/-}$ individuals was positively correlated with *CDH1* promoter hypermethylation in white-blood cells(79). We therefore hypothesized that immune activation and *CDH1* loss of function could synergise in the CLP etiology. Using human induced Pluripotent Stem Cell (hiPSC)-derived NC cells, *Xenopus* and mouse embryos, we previously showed evidence of a CLP two-hit model based on *CDH1* heterozygous loss of function and pro-inflammatory response, as genetic and environmental hits, respectively(51). However, we did not explore the maternal-fetal communication or further embryonic outcomes in the anteroposterior axis Here, we sought to investigate maternal, placental and embryonic immune responses and the repercussions on *Cdh1* expression and epigenetic landscape in the NC of mouse embryos, as well as the craniofacial development. For pro-inflammatory activation, bacterial lipopolysaccharide (LPS) was administered into adult pregnant mice, and the *Wnt1*-Cre *Cdh1*-LoxP system was used to obtain semi-floxed embryos, defined as embryos harboring one floxed *Cdh1* allele in the NC lineage.

Results

Maternal exposure to LPS induces systemic and placental pro-inflammatory response

In order to investigate the pro-inflammatory activation as an environmental factor of embryonic epigenetic regulation, intraperitoneal LPS or sterile vehicle control were injected

in pregnant females at embryonic stage E8.5. Whole maternal blood and placental tissue samples were collected 2, 4 and 24 hours after the LPS injection (Fig. 1a), as specified in Methods. To get insight into the maternal-fetal interface, we first analysed whole maternal blood Interleukin-1β (*Il-1β*), Interleukin-6 (*Il-6*) and Tumour necrosis factor alpha (*Tnf-α*) mRNA expression at 2, 6 and 24 hours after LPS administration. Two hours from LPS injection, the relative expression of *Il-6* ($p = 0.0571$) (Fig. 1b) tended to be increased up to 10^4 times, followed by all three cytokines significant expression augmentation 6 hours after the immune activation induction (Fig. 1c). No statistically relevant differences were observed at 2 or 24 hours points (Fig. 1b, 1d). Therefore, in the systemic expression profile, all three cytokines were significantly transcriptionally upregulated 6 hours after LPS exposure in maternal blood (Fig. 1e). Similarly, we found the same cytokines upregulated in placental tissue at the same 6 hours point (Fig. 1f). Confirming the transcriptional data, protein levels of IL-1β, IL-6 and TNF-α in both maternal serum and placental tissue were evaluated. Except for maternal serum TNF-α ($p = 0.3429$), all cytokines were found to be at significantly higher concentration in individuals exposed to LPS (Fig. 1g, 1h). Taken together, these results show that the treatment drives significant maternal systemic and placental immune activation detectable within 6 hours.

Impact of maternal–fetal pro-inflammatory activation on embryonic development

We sought to understand how the maternally administered insult activates the embryonic pro-inflammatory response along the anteroposterior axis, its morphological consequences on semi-floxed (*Wnt1*-Cre$^+$ *Cdh1*$^{flox/+}$) embryos, 6 hours after LPS maternal injection. LPS-treated embryos exhibited overall loose epithelial morphology (Fig. 2a), but no differences in the analysed morphometric parameters. The pharyngeal arch lateral area (PALA), crown–rump length (CRL), and abdominal antero–posterior diameter (APD) were compared (Fig. 2b). No alteration was observed in any of these features, nor were there differences in PALA relative to CRL or APD according to LPS treatment (Fig. 2c). We next investigated how the maternal pro-inflammatory activation relays to the embryo, and whether this process is related to the regulation of *Cdh1* in the context of cadherin-switch. *Il-1β*, *Il-6*, *Tnf-α* and Nuclear factor kappa B (*Nf-kB*) were evaluated in the anterior and posterior embryonic regions. *Il-6* ($p = 0.0087$) and *Tnf-α* were observed to be significantly ($p= 0.0173$) upregulated in the head, and *Il-1β* and *Nf-kB* tended to upregulation ($p = 0.0519$ and $p = 0.0519$) (Fig. 2d). Yet no differences in the expression of the same four cytokines were observed in the truncal region (Fig. 2e), suggesting that maternal immune activation affects the embryonic portions of head and trunk differently. The relative expression of genes related to the cadherin-switch and EMT (*Cdh1*, *Cdh2*, and *Zeb1*) was analyzed in the head and trunk regions. *Zeb1* is a key transcription factor controlling EMT and neural crest

specification. *Cdh1* was significantly downregulated (p = 0.0088) in the head, whereas the upregulation in *Cdh2* (p = 0.1225) did not reach statistical significance and neither *Zic1* showed to be differentially expressed between the LPS and control groups (Fig. 2f). In the trunk, no differences were observed in the expression of any of the three markers (Fig. 2g). These results indicate that the pro-inflammatory response in the proposed model is more prominent in the embryo head than in the trunk. Furthermore, this anterior-predominant response is accompanied by differential *Cdh1* expression, yet has no evident effect on the size of the first pharyngeal arch within the first few hours of inflammatory response.

Following the transcriptional analysis, we focused on the head region to determine whether E-cadherin downregulation occurs specifically at the protein level in NC cells. To address this, we measured E-cadherin protein abundance in Sox10$^+$ cells. We observed a significant decrease in the ratio of E-cadherin$^+$ to E-cadherin$^-$ cells within the Sox10$^+$ population of the LPS group (p = 0.0043); this difference was not statistically significant in the overall cell population (Fig. 3a).The proportion of Sox10+ cells was similar between the LPS and control groups (46.7% and 54.9%, respectively). However, the percentage of E-cadherin- cells was higher in the LPS group (33.1%) compared to the control (28.3%), indicating a treatment-specific effect. To rule out the possibility that the treatment altered neuroepithelial identity, we characterized the expression of key lineage markers: NC markers (*Ap2b*, *Sox10*), neural markers (*Notch1*, *Pax6*), and epithelial markers (*Cldn6*, *Krt19*). No significant differences in mRNA expression were observed between groups (Fig. 3b). We next investigated whether *Cdh1* downregulation was mediated by epigenetic mechanisms. We evaluated the mRNA expression of DNA methyltransferases (*Dnmt1*, *Dnmt3a*, *Dnmt3b*) and the histone methyltransferase *Ezh2*. Only *Dnmt3a* was transcriptionally upregulated (p = 0.0303) in LPS-treated embryos; no differences were observed for *Dnmt1*, *Dnmt3b*, or *Ezh2* (Fig. 3c). To investigate genome-wide DNA methylation changes, including those affecting Cdh1, we performed Reduced Representation Bisulfite Sequencing (RRBS). On a genome-wide scale, the LPS group exhibited 37.2% methylation in the CpG context, 3.4% in CHG (H = A, T, or C), and 2.7% in CHH, whereas the control group showed 33.8%, 3.1%, and 2.5%, respectively. The distribution of methylated CpGs revealed that 0.52% were located within CpG islands, 3.30% in shores, and 96.18% in other genomic regions. Differential methylation analysis identified 1% hypomethylated and 3% hypermethylated regions (DMRs), with their chromosomal distribution shown in Figure 5a. No significant difference in global methylation levels was detected between groups (t-test, p = 0.1091). Gene Ontology (GO) analysis of DMRs revealed enrichment for cellular component maintenance and cell junction maintenance and (Table 1). We validated *Cdh1* promoter hypermethylation by bisulfite sequencing, which showed a strong tendency towards an increased cytosine methylation (p = 0.0571) in the LPS group (n = 4) compared to the

control (n = 3). These results demonstrate that the maternal inflammatory insult alters the epigenetic landscape of *Cdh1* and affects methylation genome-wide. Furthermore, the downregulation of E-cadherin protein in neural crest cells (Fig. 3a), coupled with unchanged lineage marker expression (Fig. 3b), indicates that E-cadherin loss is a targeted event that occurs without broader changes to neuroepithelial cell identity, driven by epigenetic modifications modulated by the pro-inflammatory activation.

Lastly, we asked whether the combination of inflammatory insult and *Cdh1* haploinsufficiency could drive craniofacial malformations. To test this, pregnant Cre-LoxP and wild-type females were injected with LPS at E8.5, and embryos were harvested at E15.5 for morphological assessment. Semi-floxed embryos frequently exhibited neural tube closure defects (83% penetrance, 5/6), whereas this phenotype occurred at lower frequency in *Wnt1*-Cre$^+$ embryos (33% penetrance, 1/3) and was absent in wild-type controls (n=4) (Fig. 4a). In addition, semi-floxed embryos displayed severe craniofacial abnormalities, including neurocranial defects (83% penetrance, 5/6), cleft palate (50% penetrance, 3/6), and wider lip gaps (50% penetrance, 3/6) (Fig. 4a,b). Notably, morphometric analysis revealed that only semi-floxed embryos exhibited significantly wider lip gaps compared with wild-type ($p = 0.0069$), while *Wnt1*-Cre$^+$ showed intermediate lip gap sizes (Fig. 4b). Although *Wnt1*-Cre$^+$ littermates also presented wider lip gaps relative to wild-type, this difference did not reach statistical significance (Fig. 4b). Also, semi-floxed embryos were significantly smaller than wild-type, as indicated by a reduced CRL/APD ratio ($p = 0.0197$), while *Wnt1*-Cre$^+$ embryos showed intermediate values (Fig. 4c). These results indicate that the Cre driver itself may contribute to the craniofacial phenotype, whereas maternal pro-inflammatory exposure alone is insufficient to reproduce the observed defects. Taken together, our findings suggest that the combination of a genetic factor, mediated by single dose of *Cdh1* Cre-LoxP silencing, and an environmental factor, driven by maternal pro-inflammatory insult, can synergistically lead to craniofacial impairments.

Discussion

Our study demonstrates that maternal immune response affects the cranial NC and derived structures, and replicates the *Cdh1* downregulation driven by pro-inflammatory epigenetic regulation in the placental model. By exploring the transcriptional activity of pro-inflammatory cytokines in the maternal, placental and embryonic immune response, we demonstrated its systemic response throughout time in pregnant females as well as the embryonic consequences in the anteroposterior axis. Considering the CLP families carrying pathogenic *CDH1* variants that provided the initial evidence for this line of research, placental transmission of immune activation, and its relay to the embryo as an environmental

factor that downregulates *Cdh1*/E-cadherin in cranial NC cells through broad epigenetic modulation of cell-junction pathways, represents a key step in supporting our hypothesis.

Through comparative mRNA expression and cytokine quantification, we observed the peak of maternal systemic pro-inflammatory activation 6 hours after LPS induction. In most studies involving LPS treatment in mice, samples are harvested within the first 4 hours, which is a well-established time to investigate inflammatory outcomes(80–82), with a few ones also interested in a longer observation as we were(83,84). Intrauterine embryogenesis is thought to require maternal immunological adaptation as the fetus, a genetically distinct individual, must be supported to grow inside the pregnant female body(85) and a few studies have focused on the characterization of those adjustments. Zöllner and collaborators reported that, in murine models of sepsis, pregnancy at E16, a stage equivalent to the third trimester of human gestation, induces an increase only in the anti-inflammatory cytokine IL-4 in maternal serum, whereas the mRNA expression of IL-10 and the pro-inflammatory cytokines IL-1β, IL-6, and TNF-α is upregulated in myocardial tissue(84). They harvested samples 6 and 12 hours after pro-inflammatory induction, and used 10 µg of LPS regardless of the maternal mass, whilst we administered it according to the animal weight (i.e. 2 µg of LPS for a 20g pregnant mouse, or 100 µg/Kg). On the other hand, Vizi and collaborators reported that also in the third semester, using 10 or 50 mg/kg of LPS and sampling after 1.5 or 4 hours, the levels of IL-6, IFN-γ and TNF-α a are increased in maternal plasma, and the anti-inflammatory IL-10 is decreased(82). They also showed that the rise in circulating TNF-α already occurs at 7–8 days of murine gestation, a stage equivalent to the first trimester of human pregnancy(82). So the results regarding immune activation changes according to the methodology and also the type and quantity of LPS used can also alter the outcomes (86,87). However, these data show that during pregnancy, the pro-inflammatory activity is settled from a different baseline than non-pregnant individuals.

Pro-inflammatory activation was induced in E8.5 embryos via maternal LPS administration, which is able to cross the placental interface(88) and known to upregulate placental TNF-α, IL-1β and IL-6(89), as well as affect epigenetic inheritance in mice(90). Timing for pro-inflammatory induction was based on the offspring average NC migration and development of the choriovitelline placenta(91–93). Although mouse embryonic development resembles human embryogenesis, there are particular properties in the placentation between the two species that should be taken into account in the interpretation of mouse-model derived evidence(93). They have similar placental composition with differences in timing and mediators of decidualization, as well as tissue organization (94–96). In mice, decidualization begins at E3.5, whereas in humans there is a predecidualization before fertilization(97). By E8, mice develop a primitive placenta that is not formed in human gestation, consisting of the juxtaposition of the yolk sac against

maternal tissues and vasculature; at E12.5 the yolk sac is displaced by the definitive placenta followed by villi vascularization and around E14.5, the syncytiotrophoblast directly receives maternal blood(97). In humans, the primitive intervillous space forms around days 8–9 of gestation, and the definitive villous structure of the placenta is established by day 21. The fetoplacental circulation becomes fully functional only between the 10th and 12th weeks, when maternal blood begins to perfuse the intervillous space(93,97).Therefore, the stage at which we administered LPS (E8.5 in mice) corresponds to the late pre-vascular phase of murine placental development, approximately equivalent to the stage preceding villous vascularization in the human placenta, around days 16–18 of gestation(93). Although we present results in a mammalian system, we do not know exactly how the induced inflammation represents a human gestational inflammatory scenario, which can be driven by non infectionary scenarios, such as diabetes and nutrition habits (98,99).

Also using the Cre-LoxP system, we have previously reported that maternally administered LPS diminishes NC migration in a *Cdh1*/E-cadherin dose dependent manner in mouse embryos and also showed that NC *Cdh1* knockout (*Wnt1*-Cre^{+} *Cdh1*$^{flox/flox}$ embryos) develops CLP phenotypes(51). We found that *Cdh1* semi-floxed embryos exposed to pro-inflammatory activation exhibited markedly worsened phenotypes, particularly involving craniofacial sctructures and neural tube development. This pattern not only reveals inherent limitations of the model but also emphasizes the wide-ranging impact of systemic immune activation. We did not explore the baseline *Cdh1* expression of this model in comparison to other lineages; however, wild-type embryos submitted to LPS treatment did not develop any observable craniofacial phenotype. Human NC migration was reported to be impaired due to interferon-β exposure(100), and Zika virus infection was shown to induce NC cytokine production(101). In cell metastasis, IL-6 enhances N-cadherin expression(102), and in CLP genes related to pro-inflammatory maintenance are significantly upregulated in child cleft mucosa(103). As reported in the mouse model, pregnancy also alters the immunological system in humans (104,105). Interestingly, it has been reported that pregnant women of black ancestry exhibit greater TNF-α production during mid-pregnancy and marginally lower IL-1 production at postpartum, in comparison to those with caucasian ancestry (106), and it is known that the frequency of CLP is lower in African populations (107). In this context, further studies with other candidate genes involved in EMT might contribute to a better understanding of its role in CLP etiology.

In the experimental conditions, no differences on neural and non-neural epithelia identity were observed, neither on morphology size and proportions. Also, since no NC markers were found differentially expressed under the pro-inflammatory insult, it is suggested that NC induction remains properly maintained in the 2-hit model, but NC migration is affected by the environmental factor, as previously reported (51). The

transcriptional activation of pro-inflammatory cytokines was more prominent in the head than in the trunk, as well as the alteration in *Cdh1* expression and DNMT activity, which could be related to the axial specificity of the impairments. The axial differential sensibility to the maternal immune activation occurs also in accordance with reported ability to reactive oxygen species generation(108), which are biologically connected processes(109). Other authors have demonstrated that the cranial NC cells are also particularly sensitive to apoptosis induced by oxidative stress(110,111). In the mammalian embryonic development, cells from the dorsal anterior ectoderm differentiate into neural plate border cells and then into cranial NC, when they go through EMT and acquire mesenchymal phenotype(112–118). NC cells migrate ventrolaterally to the pharyngeal arches and give rise to the five facial prominences: two maxillary, two mandibular and one frontonasal(118). Maxillary prominences form the upper lip, mandibular form the lower lip and jaw, whereas the frontonasal prominence forms the forehead, the nose and the top of the primitive mouth(119). Therefore, NC delamination and migration are sensitive stages of craniofacial ontogeny dependent on EMT(4,41). The cellular phenotypic transition is tightly regulated and it was shown that E-cadherin to N-cadherin switch is orchestrated by ZEB1 and β-catenin activity in other EMT models(73,120). In our study, we did not explore the dynamics involving EMT regulation further than embryonic *Zeb1* transcription, which did not show to be affected by maternal immune activation. Moreover, an E-cadherin/NF-κB regulatory loop was shown to regulate E-cadherin transcription in cancer collective cell migration(121), which is consistent with our proposed gene-environment interaction in the two-hit CLP model.

Together, Sanger sequencing and RRBS results indicate *Cdh1* promoter differential methylation under pro-inflammatory activation, as well as for genes related to cell-junction maintenance. *Dnmt3a* was shown to be upregulated from the four methylating enzymes analysed by RT-qPCR. Noteworthy, *Dnmt3b* was shown to be dispensable for mouse embryonic development elsewhere(128). The disruption of NC cells DNA methylation was shown to drive mouse orofacial clefts(129) and inflammatory response has been related to DNMT3A activity(130,131). In mouse embryonic stem cells, DNMT1 and 3A/B are necessary for CG methylation symmetry across generations of cultured cells(132). Specifically, DNMT3A/B add methyl groups to recent synthesized DNA strands(131) and DNMT1 maintains DNA methylation during cell division(133). In contrast to our findings, Purkait et al. (2022)(134) showed that pro-inflammatory activation due to *Helicobacter pylori* infection activates *EZH2* and *DNMT1* in the stomach, affecting the expression of *CDH1* among other genes in hereditary diffuse gastric cancer(128). In addition to CpG methylating enzymes, we also analysed the expression of *Ezh2*, that adds methyl groups to histone H3 and was reported by the same group to mediate pro-inflammatory induced epigenetic alterations(135,136). We found enrichment of methylation related to the *Eed*, which encodes

a core component of the Polycomb Repressive Complex 2 (PRC2), that plays a pivotal role in maintaining transcriptional repression through H3K27me3 (137). The study by Ying et al. (2019) revealed that EED promoter hypomethylation is significantly associated with colorectal cancer, with tumor tissues exhibiting markedly lower methylation levels compared to normal tissues. In EMT, EED-mediated PRC2 activity can indirectly suppress *CDH1* (E-cadherin) by recruiting EMT transcription factors like *SNAIL* and *ZEB1* to the *CDH1* promoter, thereby facilitating mesenchymal transitions (137). Lastly, *Shank3*, known for its protective effect against inflammation in neurons and associated with autism/Phelan-McDermid syndrome (OMIM #606232) (138,139), which includes craniofacial dysmorphisms (140,141), was found hypomethylated in the experimental group (142).

Considering the E-cadherin structural function in mechanical forces of cellular aggregation, the protein also plays important roles in collective cell migration in a variety of models(121–126), including in orofacial clefts(126). These are fundamental proteins of general epithelia, and inflammatory activation mediated by the placenta is thought to affect the whole embryo. Here, we did not investigate the effect of *Cdh1* loss of function in other tissues, nor investigated other genetic expression alterations induced by immune response in the etiology of CLP. Also, whether the *CDH1* hypomorphism affects NC delamination is still to be investigated, albeit the observed downregulation of Cdh1/E-cadherin is consistent with the reported NC migration impairment(51). Besides acting as an adhesion molecule, E-cadherin also participates in the Wnt pathway by interacting with catenin, which has also been related to CLP(37,78). As a complex condition that affects the most sophisticated human bone and cartilage structure, alterations in cellular cadherin profile due to immune activation, could affect several phenomena involved in craniofacial development—including cellular signalization and morphogenetic movements not necessarily related to the E-cadherin to N-cadherin switch. For example, in chicken embryo NC, pro-inflammatory activation was shown to upregulate both E-cadherin and N-cadherin(127).

Conclusions

Our findings indicate that maternal pro-inflammatory activation transmitted from pregnant mice to their offspring via placental communication results in defects of NC-derived structures and epigenetic modulation of genes involved in cell junctions. In this model, the inflammatory insult, acting as an environmental factor, predominantly impacts the anterior embryonic region, the site of critical morphogenetic processes for craniofacial development, including NC migration. This mechanism may account for the incomplete penetrance of familial CLP cases harbouring *CDH1* variants, as epigenetic modulation appears to mediate the interplay between genetic susceptibility and pro-inflammatory activation. This study demonstrates how genetic susceptibility and maternal inflammation interact in the etiology of

CLP, highlighting *CDH1* as a clinically relevant target for genetic counselling. Importantly, it provides functional evidence that maternal and placental inflammatory signaling in a mammalian model can reshape embryonic development, underscoring translational relevance and possible implications for prenatal care.

Methods

Ethics

The maintenance, procedures and experiments of mouse lineages were approved by the Research Ethics Committee from the Biosciences Institute (University of Sao Paulo, Brazil) under the protocol 394/2022. All animal procedures were performed under the Committee's ethics standards.

Neural crest–specific Cdh1 conditional heterozygous mice

To generate *Mus musculus* embryos heterozygous for *Cdh1* in neural crest (NC) cells, we crossed *Wnt1*-Cre2 mice (129S4.Cg-E2f1Tg(Wnt1-cre)2Sor/J; Strain #022137, The Jackson Laboratory, USA), which express Cre-recombinase in *Wn1*+ cells, with *Cdh1*-LoxP mice (B6.129-Cdh1^tm2Kem/J; Strain #005319, The Jackson Laboratory, USA). When specified, C57BL/6J embryos were used as wild-type controls. In this study, the genotype *Wnt1*-Cre^{+} Cdh1$^{flox/+}$ designates NC *Cdh1* heterozygous embryos, whereas *Wnt1*-Cre^{+} carriers with intact *Cdh1* alleles, considered controls. Embryonic age was estimated as E0.5 based on the detection of a copulatory plug.

Embryonic morphometric measurements

E8.75 embryo images were acquired under Leica M165 FC light microscope with Leica DFC7000 camera. The pharyngeal arch lateral area (PALA), crown-rump length (CRL) and abdominal antero-posterior diameter (APD), following what was previously described(143). E15.5 craniofacial development was assessed using ultramicrotomography (µCT). To evaluate the lip gap, we calculated the ratio of the upper lip gap to the total upper lip length, and normalized this value to the biparietal diameter (BPD). The resulting values were normalised with respect to both the CRL and the APD, in order to account for overall embryonic size and growth variability. µCT results were obtained with the SkyScan 1176 instrument, using 0.22 aluminium filter with 9 µm resolution, and 3D reconstructed using NRECON v2 software. Images were obtained using the volume rendering software CTvox v3.3.1.0 (Bruker). All measurements were performed on ImageJ software(144).

Maternal pro-inflammatory activation

For pro-inflammatory activation via maternal immune activation, pregnant mice at E8.5 were injected with 100 µg/Kg LPS from Escherichia coli 026:B6 (Invitrogen™, 00-4976-93) (145). In the control group, pregnant mice were injected with the same volume of sterile vehicle control (1X PBS). Females were placed in experimental or control groups randomly. In order to preserve the effect on pro-inflammatory activation, animals were euthanized with cervical dislocation [146–148]. Adults and embryos were genotyped by PCR with Platinum Supermix (Invitrogen™) following The Jackson Laboratories recommendations. DNA samples were extracted with NucleoSpin Tissue kit (Macherey-Nagel) and PCR products were separated with electrophoresis in 1,5% agarose gel with GelRed/BFB (1:500) in TBE buffer. Gel images were photo documented with ImageQuant Las 400 mini (GE Healthcare).

mRNA expression

The expression of NC markers, cytokines, methylating enzymes and cadherins genes were analysed with quantitative Reverse Transcription Polymerase Chain Reaction (qRT-PCR). Samples were individualised in 0.5 ml tubes from properly euthanized animals and dissected in 1X PBS. For anteroposterior analysis, the embryos were transversely sectioned just caudal to the first pharyngeal arch. NucleoSpin TriPrep kit (Macherey-Nagel) was used for RNA extraction, according to recommendations. RNA samples were quantified with spectrophotometer (Epoch, BioTek) and filtered by quality of Abs260/280 = 2 ± 0.1 and Abs260/230 = 2 ± 0.2 ratios (149). cDNA was retro-transcribed with SuperScript™ VILO™ Master Mix (ThermoFisher Scientific) using 1.5 ug of RNA per sample. Fast SYBR Green Master Mix 2X (Applied Biosystems) was used for cDNA amplification with 100nM forward and reverse, following fabricant recommendations. Primer sequences, described in Table 3 were designed in exon-exon junctions using NCBI Primer Blast. Reactions were performed in a QuantStudio 5.0 System (ThermoFisher Scientific) using standard parameters. Relative expression values were calculated as previously reported, using *Actb*, *Gapdh* or *Tbp* as endogenous control selected with NormFinder(150,151).

Cytokines quantification

We quantified cytokines concentrations in maternal serum and placental protein extractions, from properly euthanized animals, with Enzyme Linked ImmunoSorbent Assay (ELISA) technique. Whole maternal blood was incubated at RT for 30 min to clot and centrifuged for 20 min at 4ºC and 16,000xg. Serum containing supernatant was transferred to ice cold tubes and stored at -80ºC. Samples were diluted in RIPA Buffer (Thermo Fisher Scientific) (1:50). Pellets were discarded. Placentas were dissected in ice cold 1X PBS. Every 5 mg of placental tissue was transferred to ice cold 1.5 ml tubes containing 300 ul of RIPA Buffer.

Samples were homogenised with an ultrasonic sonicator processor (Heat Systems) with 12 cycles of 10s and 30s intervals, with 180W wattage and at 4ºC. Next, they were centrifuged at 16,000xg for 20 min at 4ºC. Protein containing supernatant was transferred to new ice cold tubes and stored at -80ºC. Serum and placental samples were with Pierce™ BCA Protein Assay Kit (Thermo Fisher Scientific). IL1-β, IL-6 and TNF-α levels were measured with arigoPLEX® Mouse Proinflammatory Cytokine Multiplex ELISA Kit (IL1 beta, IFN gamma, TNF alpha, IL6) kit (arigobio). Protein concentrations were estimated with optical density (OD) measured in a spectrophotometer at 450 nm(Epoch, BioTek). Experimental procedures and quantification were performed according to fabricant guidelines.

Flow cytometry

E-cadherin and Sox10 expressions were evaluated with flow cytometry. Cells were obtained as described by Ward et al. (2023) [(152)]. Briefly, dissected head embryos were dissected and tissues were incubated in 500 ul PBS 1x 450 U/ml Collagenase IV 20mM HEPES for 30 min at 37ºC and 250 rpm. Cells were separated with 70 µm filters (Corning® Falcon® Cell Strainer) and centrifuge for 5 min at 400xg and 4ºC. Single cells were fixed and permeabilized with True-Nuclear™ Transcription Factor Buffer Set (BioLegend), according to manufacturer orientation. The primary antibodies Sox10 (D5V9L) Rabbit mAb #89356 (Cell Signaling) and anti-E Cadherin antibody [M168] ARG41292 (arigobio) were used in 1:100 concentration and the secondary antibodies Anti-rabbit IgG (H+L), F(ab')2 Fragment (Alexa Fluor® 647 Conjugate) #4414 (Cell Signaling) and Anti-mouse IgG (H+L), F(ab')2 Fragment (Alexa Fluor® 488 Conjugate) #4408 (Cell Signaling) with 1:500. Analysis was performed using FlowJo™ v10.8 Software (BD Life Sciences) (153).

DNA methyltransferase activity

Embryonic DNMT3A, DNMT3B and DNMT1 activity was measured with DNMT Activity Quantification Kit *(Colorimetric)* (abcam). Single cells were obtained as described and digestion was verified with flow cytometry, as previously described (152). Supernatant was recovered and cellular dissociation was verified with flow cytometry. Next, NE-PER Nuclear and Cytoplasmic Extraction Reagents kit (Thermo Fisher Scientific) was used for nuclear fractionation and samples were quantified with *Pierce™ BCA Protein Assay Kit* (Thermo Fisher Scientific). Activity was estimated based on OD measurements at 450 nm performed in a spectrophotometer (Epoch, BioTek), according to fabricant guidelines.

DNA methylation

Reduced representation bisulfite sequencing was used for investigation of diffentialy methylated regions (DMRs). 50 ng of DNA was used for library preparation and downstream

sequencing with the Zymo-Seq RRBS Library Kit (Zymo Research). Library quality was assessed with Qubit (Thermo Fisher) and Bioanalyzer (Agilent), and paired-end sequencing was done by the Human Genome and Stem Cell Research Center sequencing service, the using a SP Reagent Kit v1.5 (100 cycles) on a NovaSeq 6000 lanes (Illumina). Quality assessment was performed using FastQC. Reads were mapped to *Mus musculus* NCBI genome (mm39), and methylation calls were extracted with Bismark 0.24.2, using bowtie and methylation extractor modes, respectively (154). Differentially methylated regions (DMRs) were identified with methylkit 3.21 (155), using NCBI RefSeq mm39 genome as reference, 25% as threshold and $p < 0.001$ as criteria for relevance. Finally, DMRs were analysed in the online platform WebGestalt for biological interpretation; GO were enriched when $p < 0.05$ (156). Bisulfite Sanger sequencing was used for assessing *Cdh1* promoter methylation with bisulfite-specific primers designed on MethPrimer (157) (Table 2). DNA samples were extracted from the head of E8.75 mouse embryos using NucleoSpin TriPrep kit (Macherey-Nagel) and 200 ng of DNA per individual was converted using BisulFlash DNA Modification Kit (EpigenTek). Amplicons were purified with Sephadex LH-20 (GE Healthcare) and Sanger sequencing was performed at the Human Genome and Stem Cell Research Center. Cytosine peak values in CpGs were called using Sequencher® DNA sequence analysis software (Gene Codes Corporation) (158) and C signals were used to determine the methylation percentage as in $100 * C/(C + T)$.

Statistical analysis

Experimental data was tested for normal distribution in Prism 7 (GraphPad). Normal distributed datasets were compared with unpaired two-tailed Student's t-tests. Comparisons of non-normal distributed datasets were performed using two-tailed Mann–Whitney U-tests. 5% significance was used. Asterisks of statistical significance (**$p < 0.01$, and *$p < 0.05$) or not significant (NS) refer to a comparison with the control, unless otherwise indicated. Embryonic, placental and blood-derived samples were allocated into experimental groups according to LPS administration. No predetermination of sample sizes was performed.

Financial support

This study was supported by the National Council for Scientific and Technological Development (CNPq) and the São Paulo Research Foundation (FAPESP, 2022/07972-7; CEPID-FAPESP, 2013/08028-1).

Conflict of interest statement

The authors declare no conflict of interest.

Author contributions

DN, LA, and MRPB contributed to conceptualization, methodology, formal analysis, and interpretation of results. HMSB was responsible for animal maintenance, and ECML performed genotyping. DN carried out the investigation, collected the data, and prepared the original draft of the manuscript. DN, LA, and MRPB contributed to review and editing of the final version.

Acknowledgement

We express our gratitude for Dr. José Carlos Farias Alves Filho for discussions on experimental designs and results. We also thank Dr. Maria Fernanda Castro-Amarante for flow cytometry experiments assistance, Dr. Simone Gomes Ferreira for µCT acquisitions and reconstruction, and the Human Genome and Stem Cell Research Center sequencing service.

Figures and tables

Figure 1. LPS activates systemic and placental pro-inflammatory cytokine expression. **a** Experimental design throughout embryonic development. The copulatory plug marked stage E0.5; LPS was administered at E8.5; pro-inflammatory response was assessed 2, 6 and 24 hours later. Maternal whole blood cytokine expression post LPS injection: **b** 2 hours post LPS injection: no statistically significant differences observed. **c** 6 hours post LPS: *Il-1β* ($p = 0.0025$), *Il-6* ($p = 0.0025$), and *Tnf-α* ($p = 0.0480$) were upregulated in the LPS group **d** 24 hours post LPS: no statistically significant differences observed. **e** Overview of maternal cytokine expression shows a peak at 6 h post LPS, expressed as LPS/control mRNA fold change. **f** Pro-inflammatory cytokine expression in the placenta 6 hours post LPS injection ($n(Ctrl) = 5$, $n(LPS) = 6$): *Il-1β* ($p =0.03571$), *Il-6* ($p = 0.0357$) and *Tnf-α* ($p = 0.0480$) were upregulated in LPS-treated individuals. **g** Maternal serum cytokine levels 6 h post LPS ($n(Ctrl) = 4$, $n(LPS) = 6$): IL-1β ($p = 0.0095$) and IL-6 ($p = 0.0095$) were significantly increased, with a trend for TNF-α. **h** Placental cytokine levels 6 h post LPS ($n(Ctrl) = 5$, $n(LPS) = 6$): IL-1β ($p = 0.0043$), IL-6 ($p = 0.0043$), and TNF-α ($p = 0.0303$) were significantly

increased. Boxplot whiskers represent minimum to maximum values; in bar plots, lines indicate mean ± standard deviation.

Figure 2. Maternal pro-inflammatory activation induces embryonic axial differences in cytokine and *Cdh1* expression. **a** Embryo morphology under light microscopy shows looser epithelial structure in LPS-treated individuals. **b** Morphometric parameters: first pharyngeal arch lateral area (PALA, black hatched circle), crown–rump length (CRL, grey vertical line), and abdominal antero-posterior diameter (APD, grey horizontal line). **c** Quantification of embryo and first pharyngeal arch size: no differences between LPS and control groups in CRL/APD ratio or PALA. **d** Head pro-inflammatory cytokine expression: *Il-6* ($p = 0.0087$) and *Tnf-α* ($p = 0.0173$) were significantly upregulated; *Il-1β* and *Nf-κB* showed a trend towards upregulation. **e** Trunk pro-inflammatory cytokine expression: no significant differences observed. **f** Head expression of cadherin-switch–related genes: *Cdh1* was significantly downregulated ($p = 0.0087$), while *Cdh2* and *Zeb1* showed no significant differences. **g** Trunk expression of cadherin-switch–related genes: no significant differences in *Cdh1*, *Cdh2*, or *Zeb1*. Lines indicate median and 95% CI; boxplot whiskers represent minimum to maximum values.

Figure 3. Pro-inflammatory response in the embryo head epigenetically downregulates neural crest *Cdh1*/E-cadherin. **a** E-cadherin protein levels in neural crest and head region cells: the E-cadherin+/E-cadherin− ratio was significantly decreased in Sox10+ cells ($p = 0.0043$), while no significant difference was observed for all analysed cells. In the heat map, E-cadherin and Sox10 are displayed on the x- and y-axes, respectively. **b** *Cdh1* promoter methylation tends to be higher in the LPS group. **c** Expression of neuroepithelium markers: no significant changes in LPS/control fold change. **d** Expression of methyltransferases: only *Dnmt3a* was significantly upregulated ($p = 0.0269$). **e** Nuclear DNMT activity in LPS-treated embryos was not significantly different from controls.

Lines indicate median and 95% CI; boxplot whiskers represent minimum to maximum values; column lines indicate mean ± SD.

Figure 4. *Cdh1* single dose silencing, in combination with pro-inflammatory insult, drives craniofacial and neural tube malformations. **a** Craniofacial and neural tube defects induced by LPS in *Wnt1*-Cre^{+} *Cdh1*$^{flox/+}$ embryos (n = 6) include neural tube enclosure defects (83% penetrance), neurocranium malformations (83%), increased lip gap size (50%), and cleft palate (50%). In *Wnt1*-Cre+ embryos, neural tube enclosure defects were observed with 33% penetrance. **b** Lip gap size showed to be greatly increased in *Wnt1*-Cre^{+} *Cdh1*$^{flox/+}$ in comparison to the wild-type. **c** Embryo size showed to be decreased in *Wnt1*-Cre^{+} *Cdh1*$^{flox/+}$ in comparison to the wild-type. Lines indicate median and 95% CI.

Table 1. Top 10 enriched biological processes (GO terms) identified by WebGestalt for differentially methylated regions (DMRs) in head tissue, in LPS-treated Cdh1 semi-floxed embryos relative to controls.

Identification	Description	Number of genes	Genes of interest	P-value
GO:0098880	maintenance of postsynaptic specialization structure	21	*Dlg4*; *Shank3*; *Dlgap1*; *Syngap1*	< 0.001
GO:0099558	maintenance of synapse structure	38	*Dlg4*; *Shank3*; *Dlgap1*; *Syngap1*	0.0012
GO:0097106	postsynaptic density organization	40	*Dlg4*; *Shank3*; *Dlgap1*; *Syngap1*	0.0014
GO:0099084	postsynaptic specialization organization	46	*Dlg4*; *Shank3*; *Dlgap1*; *Syngap1*	0.0026
GO:0034331	cell junction maintenance	48	*Dlg4*; *Shank3*; *Dlgap1*; *Syngap1*	0.003
GO:0099562	maintenance of postsynaptic density structure	13	*Dlg4*; *Shank3*; *Dlgap1*	0.005
GO:0043954	cellular component maintenance	68	*Dlg4*; *Shank3*; *Dlgap1*;	< 0.001

			Syngap1	
GO:0048169	regulation of long-term neuronal synaptic plasticity	31	*Dlg4*; *Shank3*; *Syngap1*	< 0.001
GO:2000821	regulation of grooming behavior	4	*Dlg4*; *Shank3*	< 0.001
GO:0106104	regulation of glutamate receptor clustering	6	*Dlg4*; *Shank3*	< 0.001

Table 2. Primer sequences used for qRT-PCR assays.

Gene	Forward sequence (5'->3')	Reverse sequence (5'->3')
Il1-β	TGCCACCTTTTGACAGTGATG	AAGGTCCACGGGAAAGACAC
Il-6	TGATGGATGCTACCAAACTGGA	TTGGAAATTGGGGTAGGAAGGAC
Tnf-α	CAAAATTCGAGTGACAAGCCT	TGTCTTTGAGATCCATGCCGT
Nf-kB	CAGAGGCGTGTATTAGGGGC	GCATTCGGGGCTTTGCTATC
Dnmt1	TGGTCTTCCCCCACTCTCTTG	TGTTAAGCCATCTCTTTCCAAGTC
Dnmt3a	TGCTTACAAAGACCACGGCA	CCTGTTCCTCTCCTTCCTTTCG
Dnmt3b	CTGGAAGAATTTGAGCCACCCA	GAGCACCAAGTACCCCGTTG
Ezh2	CCATGCAACACCCAACACATA	CTTAGCTCCCTCCAGATGCT
Cdh1	CGCCACAGATGATGGTTCAC	GCAGTAAAGGGGGACGTGTT
Cdh2	AGCCCGGTTTCACTTGAGAG	TCATCCGCATCAATGGCAGT
Zeb1	GCTGGCAAGACAACGTGAAA	TCACAATACGGGCAGGTGAG
Actb	GGGTATCTGCTGGCGGTTT	GGCCAAGCCCTGAGCATAAG
Cldn6	AGTCTCTTTTGCAGGCTCG	TCCCCAAGATTTGCAGACCAG
Krt19	AGGTGAAGATCCGCGACTGG	CGTGTTCTGTCTCAAACTTGGTTCT
Ap2b	CCTCACTGGTAGAAGGGGAAG	TCAAATACTCGGACACGGCTT
Sox10	CTAGCCGACCAGTACCCTCA	ACTTTCGTTCAGCAACCTCCA
Notch1	AGGCTTCAGTGGCCCTAAT	TGCATACCCCGCTGTTTTTG
Pax6	TTGAGAAGTGTGGGAACCAGC	CACTCCGCTGTGACTGTTCTG
Gapdh	CCCAGCTTAGGTTCATCAGGTAA	TGTGCCGTTGAATTTGCCG
Tbp	GGGTATCTGCTGGCGGTTT	GGCCAAGCCCTGAGCATAAG

Table 3. Pair of primers used for *Cdh1* promoter bisulfite PCR and Sanger sequencing.

Forward sequence (5'->3')	Reverse sequence (5'->3')
TAAGGGAAACTGATGGTGTTACT	AATACCGATGACCTCTAAATACCCT

References

1. Fitzsimons KJ, Hamilton MJ, van der Meulen J, Medina J, Wahedally M, Park MH, et al. Range and Frequency of Congenital Malformations Among Children With Cleft Lip and/or Palate. Cleft Palate Craniofac J. 2023 Aug;60(8):917–27.
2. Mc Goldrick N, Revie G, Groisman B, Hurtado-Villa P, Sipek A, Khoshnood B, et al. A multi-program analysis of cleft lip with cleft palate prevalence and mortality using data from 22 International Clearinghouse for Birth Defects Surveillance and Research programs, 1974-2014. Birth Defects Res. 2023 Jun 1;115(10):980–97.
3. Kantar RS, Hamdan US, Muller JN, Hemal K, Younan RA, Haddad M, et al. Global prevalence and burden of orofacial clefts: A systematic analysis for the global burden of disease study 2019. J Craniofac Surg. 2023 Oct 1;34(7):2012–5.
4. Bernheim N, Georges M, Malevez C, De Mey A, Mansbach A. Embryology and epidemiology of cleft lip and palate. B-ENT. 2006;2 Suppl 4:11–9.
5. Wehby GL, Cassell CH. The impact of orofacial clefts on quality of life and healthcare use and costs. Oral Dis. 2010 Jan;16(1):3–10.
6. Zeytinoglu S, Davey MP. It's a privilege to smile: impact of cleft lip palate on families. Fam Syst Health. 2012 Sep;30(3):265–77.
7. Glener AD, Allori AC, Shammas RL, Carlson AR, Pien IJ, Aylsworth AS, et al. A Population-Based Exploration of the Social Implications Associated with Cleft Lip and/or Palate. Plast Reconstr Surg Glob Open. 2017 Jun 29;5(6):e1373.
8. Apon I, van Leeuwen N, Polinder S, Versnel SL, Wolvius EB, Koudstaal MJ. Healthcare use and direct medical costs in a cleft lip and palate population: an analysis of observed and protocolized care and costs. Int J Oral Maxillofac Surg. 2024 Apr;53(4):286–92.
9. MacLean JE, Fitzsimons D, Fitzgerald DA, Waters KA. The spectrum of sleep-disordered breathing symptoms and respiratory events in infants with cleft lip and/or palate. Arch Dis Child. 2012 Dec;97(12):1058–63.
10. Lindberg NE, Kynø NM, Feragen KB, Pripp AH, Tønseth KA. Parental Stress, Infant Feeding and Well-being in Families Affected by Cleft Lip and/or Cleft Palate: The Impact of Early Follow-up. Cleft Palate Craniofac J. 2024 Feb 21;10556656241231524.
11. Miller S, Kallusky J, Zimmerer R, Tavassol F, Gellrich N-C, Ptok M, et al. Differences in velopharyngeal pressures during speech sound production in patients with unilateral cleft lip and palate (UCLP) and healthy individuals. Ger Med Sci. 2024 Mar 1;22:Doc02.
12. Wells-Durand E, Buchel A, Tuen YJ, Thomson R, Staples J, Gibson TL, et al. What Does Cleft Lip and Palate Care Cost? The Time and Economic-Associated Burden of Care From Birth to Maturity. Plast Surg (Oakv). 2023 Oct 9;
13. Trezza PM, Gimenes RMT, Costa CKF, Massuda EM. Custo do Tratamento Complementar da Fissura Labiopalatina. UNINGÁ. 2016 Jan 19;47:38–44.
14. Martinelli M, Palmieri A, Carinci F, Scapoli L. Non-syndromic Cleft Palate: An

Overview on Human Genetic and Environmental Risk Factors. Front Cell Dev Biol. 2020 Oct 20;8:592271.

15. Stone C. Cleft Lip and Palate: Etiology, Epidemiology, Preventive and Intervention Strategies. Anat Physiol. 2013;04(03).

16. Reynolds K, Kumari P, Sepulveda Rincon L, Gu R, Ji Y, Kumar S, et al. Wnt signaling in orofacial clefts: crosstalk, pathogenesis and models. Dis Model Mech. 2019 Feb 4;12(2).

17. Alghonemy WY, Gaber Ashmawy M. Meta-analysis and systematic review for the genetic basis of cleft lip and palate. J Oral Biol Craniofac Res. 2025 Jan 8;15(1):146–52.

18. Fonseca-Souza G, Tessari VS, Scariot R, Kirschneck C, Coletta RD, Küchler EC, et al. Exploring polymorphisms in genes encoding growth factors associated with non-syndromic cleft lip with or without cleft palate and tooth agenesis. J Appl Oral Sci. 2025 Mar 14;33:e20240501.

19. Fu Z, Qi Y, Xue L-F, Xu Y-X, Yue J, Zhao J-Z, et al. LAMA5: a new pathogenic gene for Non-Syndromic Cleft Lip with or without Cleft Palate. Biomed J. 2023 Jun 28;100627.

20. Liu J, Chanumolu SK, White KM, Albahrani M, Otu HH, Nawshad A. Transcriptional analysis of cleft palate in TGFβ3 mutant mice. Sci Rep. 2020 Sep 10;10(1):14940.

21. Lu Y, Liang M, Zhang Q, Liu Z, Song Y, Lai L, et al. Mutations of GADD45G in rabbits cause cleft lip by the disorder of proliferation, apoptosis and epithelial-mesenchymal transition (EMT). Biochim Biophys Acta Mol Basis Dis. 2019 Sep 1;1865(9):2356–67.

22. Lara LDS, Coletta RD, Assis Machado R, Querino Rocha de Oliveira L, Martelli Júnior H, de Almeida Reis SR, et al. Exploring the role of the WNT5A rs566926 polymorphism and its interactions in non-syndromic orofacial cleft: a multicenter study in Brazil. J Appl Oral Sci. 2024 Feb 12;32:e20230353.

23. Bagordakis E, Paranaiba LMR, Brito LA, de Aquino SN, Messetti AC, Martelli-Junior H, et al. Polymorphisms at regions 1p22.1 (rs560426) and 8q24 (rs1530300) are risk markers for nonsyndromic cleft lip and/or palate in the Brazilian population. Am J Med Genet A. 2013 May;161A(5):1177–80.

24. de Araujo TK, Secolin R, Félix TM, de Souza LT, Fontes MÍB, Monlleó IL, et al. A multicentric association study between 39 genes and nonsyndromic cleft lip and palate in a Brazilian population. J Craniomaxillofac Surg. 2016 Jan;44(1):16–20.

25. Saket M, Saliminejad K, Kamali K, Moghadam FA, Anvar NE, Khorram Khorshid HR. BMP2 and BMP4 variations and risk of non-syndromic cleft lip and palate. Arch Oral Biol. 2016 Dec;72:134–7.

26. Brito LA, Yamamoto GL, Melo S, Malcher C, Ferreira SG, Figueiredo J, et al. Rare Variants in the Epithelial Cadherin Gene Underlying the Genetic Etiology of Nonsyndromic Cleft Lip with or without Cleft Palate. Hum Mutat. 2015 Nov;36(11):1029–33.

27. Frebourg T, Oliveira C, Hochain P, Karam R, Manouvrier S, Graziadio C, et al. Cleft lip/palate and CDH1/E-cadherin mutations in families with hereditary diffuse gastric cancer. J Med Genet. 2006 Feb;43(2):138–42.

28. Reis LM, Houssin NS, Zamora C, Abdul-Rahman O, Kalish JM, Zackai EH, et al. Novel variants in CDH2 are associated with a new syndrome including Peters anomaly. Clin Genet. 2020 Mar;97(3):502–8.

29. Kumari P, Singh SK, Raman R. A novel non-coding RNA within an intron of CDH2 and association of its SNP with non-syndromic cleft lip and palate. Gene. 2018 Jun 5;658:123–8.

30. Huang C, Kratzer M-C, Wedlich D, Kashef J. E-cadherin is required for cranial neural crest migration in Xenopus laevis. Dev Biol. 2016 Mar 15;411(2):159–71.

31. Hozyasz KK, Mostowska A, Wójcicki P, Lasota A, Offert B, Balcerek A, et al. Nucleotide variants of the cancer predisposing gene CDH1 and the risk of non-syndromic cleft lip with or without cleft palate. Fam Cancer. 2014 Sep;13(3):415–21.

32. Benusiglio PR, Caron O, Consolino E, Duvillard P, Coulet F, Blayau M, et al. Cleft lip, cleft palate, hereditary diffuse gastric cancer and germline mutations in CDH1. Int J Cancer. 2013 May 15;132(10):2470.

33. Theveneau E, Steventon B, Scarpa E, Garcia S, Trepat X, Streit A, et al. Chase-and-run between adjacent cell populations promotes directional collective migration. Nat Cell Biol. 2013 Jul;15(7):763–72.

34. Larue L, Ohsugi M, Hirchenhain J, Kemler R. E-cadherin null mutant embryos fail to form a trophectoderm epithelium. Proc Natl Acad Sci USA. 1994 Aug 16;91(17):8263–7.

35. Stephenson RO, Yamanaka Y, Rossant J. Disorganized epithelial polarity and excess trophectoderm cell fate in preimplantation embryos lacking E-cadherin. Development. 2010 Oct;137(20):3383–91.

36. Liu F, Millar SE. Wnt/beta-catenin signaling in oral tissue development and disease. J Dent Res. 2010 Apr;89(4):318–30.

37. Cox LL, Cox TC, Moreno Uribe LM, Zhu Y, Richter CT, Nidey N, et al. Mutations in the Epithelial Cadherin-p120-Catenin Complex Cause Mendelian Non-Syndromic Cleft Lip with or without Cleft Palate. Am J Hum Genet. 2018 Jun 7;102(6):1143–57.

38. Conti B, Di Napoli C, Hafdaoui S, Nicotra V, Cesaretti C, Runza L, et al. CTNND1-Related Disorder: New Insight on Prenatal Phenotype. Am J Med Genet A. 2025 Mar;197(3):e63921.

39. Zhao R, Trainor PA. Epithelial to mesenchymal transition during mammalian neural crest cell delamination. Semin Cell Dev Biol. 2023 Mar 30;138:54–67.

40. Minoux M, Rijli FM. Molecular mechanisms of cranial neural crest cell migration and patterning in craniofacial development. Development. 2010 Aug;137(16):2605–21.

41. Passos-Bueno MR, Ornelas CC, Fanganiello RD. Syndromes of the first and second pharyngeal arches: A review. Am J Med Genet A. 2009 Aug;149A(8):1853–9.

42. Hansford S, Kaurah P, Li-Chang H, Woo M, Senz J, Pinheiro H, et al. Hereditary diffuse gastric cancer syndrome: CDH1 mutations and beyond. JAMA Oncol. 2015 Apr;1(1):23–32.

43. Taja-Chayeb L, Vidal-Millán S, Trejo-Becerril C, Pérez-Cárdenas E, Chávez-Blanco

A, Domínguez-Gómez G, et al. Hereditary diffuse gastric cancer (HDGC). An overview. Clin Res Hepatol Gastroenterol. 2022 Apr;46(4):101820.

44. Kievit A, Tessadori F, Douben H, Jordens I, Maurice M, Hoogeboom J, et al. Variants in members of the cadherin-catenin complex, CDH1 and CTNND1, cause blepharocheilodontic syndrome. Eur J Hum Genet. 2018 Feb;26(2):210–9.

45. Ghoumid J, Stichelbout M, Jourdain A-S, Frenois F, Lejeune-Dumoulin S, Alex-Cordier M-P, et al. Blepharocheilodontic syndrome is a CDH1 pathway-related disorder due to mutations in CDH1 and CTNND1. Genet Med. 2017 Sep;19(9):1013–21.

46. Pereira CK, Nascimento NL, Miguel AFP, Batistella EÂ, Vieira DSC, Rivero ERC. Evaluation of epithelial-mesenchymal transition markers in oral squamous cell carcinoma. Oral Surg Oral Med Oral Pathol Oral Radiol. 2025 May;139(5):e131.

47. Corso G, Magnoni F, Dal Molin M, Marino E, Nicosia L, Pesapane F, et al. Second-hit CDH1 gene mechanisms in hereditary diffuse gastric and lobular breast cancer syndrome: frequency and impact on tumorigenesis. Hum Mol Genet. 2025 Jun 9;

48. Leathers TA, Rogers CD. Time to go: neural crest cell epithelial-to-mesenchymal transition. Development. 2022 Aug 1;149(15).

49. Pinheiro H, Bordeira-Carriço R, Seixas S, Carvalho J, Senz J, Oliveira P, et al. Allele-specific CDH1 downregulation and hereditary diffuse gastric cancer. Hum Mol Genet. 2010 Mar 1;19(5):943–52.

50. Phan J, Kulkarni A, Dubowsky A, Rawlings L, Friend K, Hardy T, et al. Clefting and cancer: A complex CDH1 case. Pathology. 2022 Mar;54:S14.

51. Alvizi L, Nani D, Brito LA, Kobayashi GS, Passos-Bueno MR, Mayor R. Neural crest E-cadherin loss drives cleft lip/palate by epigenetic modulation via pro-inflammatory gene-environment interaction. Nat Commun. 2023 May 24;14(1):2868.

52. Girirajan S, Rosenfeld JA, Cooper GM, Antonacci F, Siswara P, Itsara A, et al. A recurrent 16p12.1 microdeletion supports a two-hit model for severe developmental delay. Nat Genet. 2010 Mar;42(3):203–9.

53. Kumar RA. Two-hit wonder: a novel genetic model to explain variable expressivity in severe pediatric phenotypes. Clin Genet. 2010 Dec;78(6):517–9.

54. Maynard TM, Sikich L, Lieberman JA, LaMantia AS. Neural development, cell-cell signaling, and the “two-hit” hypothesis of schizophrenia. Schizophr Bull. 2001;27(3):457–76.

55. Canicatti V, Cibin V, Berardi N, Bozzi Y, Sale A, Chelini G. Automated assessment of the mouse body-language reveals pervasive behavioral disruption in a two-hit model of psychiatric vulnerability. BioRxiv. 2025 Feb 5;

56. DeBose-Scarlett E, Ressler AK, Friday C, Prickett KK, Roberts JW, Gossage JR, et al. Arteriovenous malformation from a patient with JP-HHT harbours two second-hit somatic DNA alterations in SMAD4. J Med Genet. 2025 Mar 20;62(4):281–8.

57. Mao K, Borel C, Ansar M, Jolly A, Makrythanasis P, Froehlich C, et al. FOXI3 pathogenic variants cause one form of craniofacial microsomia. Nat Commun. 2023 Apr 11;14(1):2026.

58. Vo HDL, Lovely CB. Ethanol Induces Craniofacial Defects in Bmp Mutants Independent of nkx2.3 by Elevating Cranial Neural Crest Cell Apoptosis. Biomedicines. 2025 Mar 20;13(3).

59. Trainor P. Neural Crest Cells: Evolution, Development and Disease. 1st ed. Amsterdam: Academic Press; 2013.

60. Tolarová MM, Cervenka J. Classification and birth prevalence of orofacial clefts. Am J Med Genet. 1998 Jan 13;75(2):126–37.

61. Johnston MC, Bronsky PT. Animal models for human craniofacial malformations. J Craniofac Genet Dev Biol. 1991 Dec;11(4):277–91.

62. Murillo C, Rueda C, Larroya M, Boada D, Grau L, Ponce J, et al. Intra-amniotic infection and/or inflammation is associated with fetal cardiac concentric hypertrophy and diastolic dysfunction in preterm labor and preterm prelabor rupture of membranes. Am J Obstet Gynecol. 2024 Jan 9;

63. Parisi F, Milazzo R, Savasi VM, Cetin I. Maternal Low-Grade Chronic Inflammation and Intrauterine Programming of Health and Disease. Int J Mol Sci. 2021 Feb 9;22(4).

64. Bell MJ, Hallenbeck JM. Effects of intrauterine inflammation on developing rat brain. J Neurosci Res. 2002 Nov 15;70(4):570–9.

65. Acs N, Bánhidy F, Puhó E, Czeizel AE. Maternal influenza during pregnancy and risk of congenital abnormalities in offspring. Birth Defects Res Part A Clin Mol Teratol. 2005 Dec;73(12):989–96.

66. Shahrukh Hashmi S, Gallaway MS, Waller DK, Langlois PH, Hecht JT, National Birth Defects Prevention Study. Maternal fever during early pregnancy and the risk of oral clefts. Birth Defects Res Part A Clin Mol Teratol. 2010 Mar;88(3):186–94.

67. Carter TC, Olney RS, Mitchell AA, Romitti PA, Bell EM, Druschel CM, et al. Maternal self-reported genital tract infections during pregnancy and the risk of selected birth defects. Birth Defects Res Part A Clin Mol Teratol. 2011 Feb;91(2):108–16.

68. Waller DK, Hashmi SS, Hoyt AT, Duong HT, Tinker SC, Gallaway MS, et al. Maternal report of fever from cold or flu during early pregnancy and the risk for noncardiac birth defects, National Birth Defects Prevention Study, 1997-2011. Birth Defects Res. 2018 Mar 1;110(4):342–51.

69. Shi F-P, Huang Y-Y, Dai Q-Q, Chen Y-L, Jiang H-Y, Liang S-Y. Maternal Common Cold or Fever During Pregnancy and the Risk of Orofacial Clefts in the Offspring: A Systematic Review and Meta-analysis. Cleft Palate Craniofac J. 2023 Apr;60(4):446–53.

70. Heydari M-H, Sadeghian A, Khadivi G, Mustafa HJ, Javinani A, Nadjmi N, et al. Prevalence, trend, and associated risk factors for cleft lip with/without cleft palate: a national study on live births from 2016 to 2021. BMC Oral Health. 2024 Jan 7;24(1):36.

71. Shull LC, Artinger KB. Epigenetic regulation of craniofacial development and disease. Birth Defects Res. 2024 Jan;116(1):e2271.

72. Zhou J, Zhang C, Pan J, Chen L, Qi S-T. Interleukin-6 induces an

epithelial-mesenchymal transition phenotype in human adamantinomatous craniopharyngioma cells and promotes tumor cell migration. Mol Med Report. 2017 Jun;15(6):4123–31.

73. Gu K, Li M-M, Shen J, Liu F, Cao J-Y, Jin S, et al. Interleukin-17-induced EMT promotes lung cancer cell migration and invasion via NF-κB/ZEB1 signal pathway. Am J Cancer Res. 2015 Feb 15;5(3):1169–79.

74. Debelec-Butuner B, Alapinar C, Ertunc N, Gonen-Korkmaz C, Yörükoğlu K, Korkmaz KS. TNFα-mediated loss of β-catenin/E-cadherin association and subsequent increase in cell migration is partially restored by NKX3.1 expression in prostate cells. PLoS ONE. 2014 Oct 31;9(10):e109868.

75. Saito T, Yoshida K, Matsumoto K, Saeki K, Tanaka Y, Ong S-M, et al. Inflammatory cytokines induce a reduction in E-cadherin expression and morphological changes in MDCK cells. Res Vet Sci. 2014 Apr;96(2):288–91.

76. Jee YS, Jang TJ, Jung KH. Prostaglandin E(2) and interleukin-1β reduce E-cadherin expression by enhancing snail expression in gastric cancer cells. J Korean Med Sci. 2012 Sep;27(9):987–92.

77. Qian X, Huang C, Cho CH, Hui WM, Rashid A, Chan AOO. E-cadherin promoter hypermethylation induced by interleukin-1beta treatment or H. pylori infection in human gastric cancer cell lines. Cancer Lett. 2008 May 8;263(1):107–13.

78. Brito LA, Cruz LA, Rocha KM, Barbara LK, Silva CBF, Bueno DF, et al. Genetic contribution for non-syndromic cleft lip with or without cleft palate (NS CL/P) in different regions of Brazil and implications for association studies. Am J Med Genet A. 2011 Jul;155A(7):1581–7.

79. Alvizi L, Ke X, Brito LA, Seselgyte R, Moore GE, Stanier P, et al. Differential methylation is associated with non-syndromic cleft lip and palate and contributes to penetrance effects. Sci Rep. 2017 May 26;7(1):2441.

80. Nugraha G, Shodiq M, Misutarno, Putri RA, Noventi I, Rohmawati R. Induction of Lipopolysaccharide During Pregnancy Will Suppress IL-6 Production but not Activin B. RGSA. 2024 Mar 21;18(5):e05586.

81. Fidel PL, Romero R, Wolf N, Cutright J, Ramirez M, Araneda H, et al. Systemic and local cytokine profiles in endotoxin-induced preterm parturition in mice. Am J Obstet Gynecol. 1994 May;170(5 Pt 1):1467–75.

82. Vizi ES, Szelényi J, Selmeczy ZS, Papp Z, Németh ZH, Haskó G. Enhanced tumor necrosis factor-alpha-specific and decreased interleukin-10-specific immune responses to LPS during the third trimester of pregnancy in mice. J Endocrinol. 2001 Nov;171(2):355–61.

83. Sze MA, Tsuruta M, Yang S-WJ, Oh Y, Man SFP, Hogg JC, et al. Changes in the bacterial microbiota in gut, blood, and lungs following acute LPS instillation into mice lungs. PLoS ONE. 2014 Oct 21;9(10):e111228.

84. Zöllner J, Howe LG, Edey LF, O'Dea KP, Takata M, Gordon F, et al. The response of the innate immune and cardiovascular systems to LPS in pregnant and nonpregnant mice. Biol Reprod. 2017 Aug 1;97(2):258–72.

85. Tang M-X, Hu X-H, Liu Z-Z, Kwak-Kim J, Liao A-H. What are the roles of

macrophages and monocytes in human pregnancy? J Reprod Immunol. 2015 Nov;112:73–80.

86. Edey LF, O'Dea KP, Herbert BR, Hua R, Waddington SN, MacIntyre DA, et al. The local and systemic immune response to intrauterine LPS in the prepartum mouse. Biol Reprod. 2016 Dec;95(6):125.

87. Migale R, Herbert BR, Lee YS, Sykes L, Waddington SN, Peebles D, et al. Specific lipopolysaccharide serotypes induce differential maternal and neonatal inflammatory responses in a murine model of preterm labor. Am J Pathol. 2015 Sep;185(9):2390–401.

88. Brown AG, Maubert ME, Anton L, Heiser LM, Elovitz MA. The tracking of lipopolysaccharide through the feto-maternal compartment and the involvement of maternal TLR4 in inflammation-induced fetal brain injury. Am J Reprod Immunol. 2019 Dec;82(6):e13189.

89. Kwon H-K, Choi GB, Huh JR. Maternal inflammation and its ramifications on fetal neurodevelopment. Trends Immunol. 2022 Mar;43(3):230–44.

90. Kim S, Yoneda E, Tomita K, Kayano M, Watanabe H, Sasaki M, et al. LPS Administration during Fertilization Affects Epigenetic Inheritance during Embryonic Development. Animals (Basel). 2023 Mar 23;13(7).

91. Wilson YM, Richards KL, Ford-Perriss ML, Panthier J-J, Murphy M. Neural crest cell lineage segregation in the mouse neural tube. Development. 2004 Dec;131(24):6153–62.

92. Trainor PA. Specification of neural crest cell formation and migration in mouse embryos. Semin Cell Dev Biol. 2005 Dec;16(6):683–93.

93. Ander SE, Diamond MS, Coyne CB. Immune responses at the maternal-fetal interface. Sci Immunol. 2019 Jan 11;4(31).

94. Noyes RW, Hertig AT, Rock J. Dating the endometrial biopsy. Am J Obstet Gynecol. 1975 May;122(2):262–3.

95. Adamson SL, Lu Y, Whiteley KJ, Holmyard D, Hemberger M, Pfarrer C, et al. Interactions between trophoblast cells and the maternal and fetal circulation in the mouse placenta. Dev Biol. 2002 Oct 15;250(2):358–73.

96. Pijnenborg R, Vercruysse L, Hanssens M. The uterine spiral arteries in human pregnancy: facts and controversies. Placenta. 2006 Feb 20;27(9–10):939–58.

97. Malassiné A, Frendo JL, Evain-Brion D. A comparison of placental development and endocrine functions between the human and mouse model. Hum Reprod Update. 2003;9(6):531–9.

98. Ornoy A, Becker M, Weinstein-Fudim L, Ergaz Z. Diabetes during Pregnancy: A Maternal Disease Complicating the Course of Pregnancy with Long-Term Deleterious Effects on the Offspring. A Clinical Review. Int J Mol Sci. 2021 Mar 15;22(6).

99. Kutbi H, Wehby GL, Moreno Uribe LM, Romitti PA, Carmichael S, Shaw GM, et al. Maternal underweight and obesity and risk of orofacial clefts in a large international consortium of population-based studies. Int J Epidemiol. 2017 Feb 1;46(1):190–9.

100. Pallocca G, Nyffeler J, Dolde X, Grinberg M, Gstraunthaler G, Waldmann T, et al.

Impairment of human neural crest cell migration by prolonged exposure to interferon-beta. Arch Toxicol. 2017 Oct;91(10):3385–402.

101. Bayless NL, Greenberg RS, Swigut T, Wysocka J, Blish CA. Zika virus infection induces cranial neural crest cells to produce cytokines at levels detrimental for neurogenesis. Cell Host Microbe. 2016 Oct 12;20(4):423–8.

102. Na Y-R, Lee J-S, Lee S-J, Seok S-H. Interleukin-6-induced Twist and N-cadherin enhance melanoma cell metastasis. Melanoma Res. 2013 Dec;23(6):434–43.

103. Jain N, Pilmane M. Evaluating the Expression of Candidate Homeobox Genes and Their Role in Local-Site Inflammation in Mucosal Tissue Obtained from Children with Non-Syndromic Cleft Lip and Palate. J Pers Med. 2021 Nov 2;11(11).

104. Liu S, Diao L, Huang C, Li Y, Zeng Y, Kwak-Kim JYH. The role of decidual immune cells on human pregnancy. J Reprod Immunol. 2017 Nov;124:44–53.

105. Hsu P, Nanan RKH. Innate and adaptive immune interactions at the fetal-maternal interface in healthy human pregnancy and pre-eclampsia. Front Immunol. 2014 Mar 28;5:125.

106. Gillespie SL, Porter K, Christian LM. Adaptation of the inflammatory immune response across pregnancy and postpartum in Black and White women. J Reprod Immunol. 2016 Apr;114:27–31.

107. Mossey PA, Modell B. Epidemiology of oral clefts 2012: an international perspective. Front Oral Biol. 2012 Jun 25;16:1–18.

108. Agharazii M, St-Louis R, Gautier-Bastien A, Ung R-V, Mokas S, Larivière R, et al. Inflammatory cytokines and reactive oxygen species as mediators of chronic kidney disease-related vascular calcification. Am J Hypertens. 2015 Jun;28(6):746–55.

109. Ko E-Y, Cho S-H, Kwon S-H, Eom C-Y, Jeong MS, Lee W, et al. The roles of NF-κB and ROS in regulation of pro-inflammatory mediators of inflammation induction in LPS-stimulated zebrafish embryos. Fish Shellfish Immunol. 2017 Sep;68:525–9.

110. Sakai D, Dixon J, Achilleos A, Dixon M, Trainor PA. Prevention of Treacher Collins syndrome craniofacial anomalies in mouse models via maternal antioxidant supplementation. Nat Commun. 2016 Jan 21;7:10328.

111. Sakai D, Trainor PA. Face off against ROS: Tcof1/Treacle safeguards neuroepithelial cells and progenitor neural crest cells from oxidative stress during craniofacial development. Dev Growth Differ. 2016 Sep;58(7):577–85.

112. Lan Y, Jiang R. Mouse models in palate development and orofacial cleft research: Understanding the crucial role and regulation of epithelial integrity in facial and palate morphogenesis. Curr Top Dev Biol. 2022 Feb 28;148:13–50.

113. Williams RM, Lukoseviciute M, Sauka-Spengler T, Bronner ME. Single-cell atlas of early chick development reveals gradual segregation of neural crest lineage from the neural plate border during neurulation. eLife. 2022 Jan 28;11.

114. Szabó A, Mayor R. Mechanisms of neural crest migration. Annu Rev Genet. 2018 Nov 23;52:43–63.

115. Milet C, Monsoro-Burq AH. Neural crest induction at the neural plate border in vertebrates. Dev Biol. 2012 Jun 1;366(1):22–33.

116. Yu W, Serrano M, Miguel SS, Ruest LB, Svoboda KKH. Cleft lip and palate genetics and application in early embryological development. Indian J Plast Surg. 2009 Oct;42 Suppl:S35-50.

117. Hong C-S, Saint-Jeannet J-P. The activity of Pax3 and Zic1 regulates three distinct cell fates at the neural plate border. Mol Biol Cell. 2007 Jun;18(6):2192–202.

118. García-Castro MI, Marcelle C, Bronner-Fraser M. Ectodermal Wnt function as a neural crest inducer. Science. 2002 Aug 2;297(5582):848–51.

119. Smeriglio P, Zalc A. Cranial neural crest cells contribution to craniofacial bone development and regeneration. Curr Osteoporos Rep. 2023 Oct;21(5):624–31.

120. Wei J, Wu L, Yang S, Zhang C, Feng L, Wang M, et al. E-cadherin to N-cadherin switching in the TGF-β1 mediated retinal pigment epithelial to mesenchymal transition. Exp Eye Res. 2022 Jul;220:109085.

121. Frey N, Ouologuem L, Blenninger J, Siow W-X, Thorn-Seshold J, Stöckl J, et al. Endolysosomal TRPML1 channel regulates cancer cell migration by altering intracellular trafficking of E-cadherin and β1-integrin. J Biol Chem. 2024 Jan;300(1):105581.

122. Arslan FN, Hannezo É, Merrin J, Loose M, Heisenberg C-P. Adhesion-induced cortical flows pattern E-cadherin-mediated cell contacts. Curr Biol. 2024 Jan 8;34(1):171-182.e8.

123. Lu Y-W, Hou X-L, Koo H-M, Chao W-T. Dasatinib suppresses collective cell migration through the coordination of focal adhesion and E-cadherin in colon cancer cells. Heliyon. 2024 Jan 15;10(1):e23501.

124. Lu H, Cao LL, Ballout F, Belkhiri A, Peng D, Chen L, et al. Reflux conditions induce E-cadherin cleavage and EMT via APE1 redox function in oesophageal adenocarcinoma. Gut. 2023 Dec 7;73(1):47–62.

125. Scarpa E, Szabó A, Bibonne A, Theveneau E, Parsons M, Mayor R. Cadherin Switch during EMT in Neural Crest Cells Leads to Contact Inhibition of Locomotion via Repolarization of Forces. Dev Cell. 2015 Aug 24;34(4):421–34.

126. Pereira J, Melo S, Ferreira RM, Carneiro P, Yang V, Maia AF, et al. E-cadherin variants associated with oral facial clefts trigger aberrant cell motility in a REG1A-dependent manner. Cell Commun Signal. 2024 Feb 27;22(1):152.

127. Li H, Long D, Lv G, Cheng X, Wang G, Yang X. The double-edged sword role of TGF-β signaling pathway between intrauterine inflammation and cranial neural crest development. FASEB J. 2022 Jan;36(1):e22113.

128. Jacques-Fricke BT, Roffers-Agarwal J, Gammill LS. DNA methyltransferase 3b is dispensable for mouse neural crest development. PLoS ONE. 2012 Oct 18;7(10):e47794.

129. Ulschmid CM, Sun MR, Jabbarpour CR, Steward AC, Rivera-González KS, Cao J, et al. Disruption of DNA methylation-mediated cranial neural crest proliferation and differentiation causes orofacial clefts in mice. Proc Natl Acad Sci USA. 2024 Jan 16;121(3):e2317668121.

130. Liao M, Chen R, Yang Y, He H, Xu L, Jiang Y, et al. Aging-elevated inflammation

promotes DNMT3A R878H-driven clonal hematopoiesis. Acta Pharm Sin B. 2022 Feb;12(2):678–91.

131. Leoni C, Montagner S, Rinaldi A, Bertoni F, Polletti S, Balestrieri C, et al. Dnmt3a restrains mast cell inflammatory responses. Proc Natl Acad Sci USA. 2017 Feb 21;114(8):E1490–9.

132. Li Z, Dai H, Martos SN, Xu B, Gao Y, Li T, et al. Distinct roles of DNMT1-dependent and DNMT1-independent methylation patterns in the genome of mouse embryonic stem cells. Genome Biol. 2015 Jun 2;16(1):115.

133. Bostick M, Kim JK, Estève P-O, Clark A, Pradhan S, Jacobsen SE. UHRF1 plays a role in maintaining DNA methylation in mammalian cells. Science. 2007 Sep 21;317(5845):1760–4.

134. Purkait S, Patra S, Mitra S, Behera MM, Panigrahi MK, Kumar P, et al. Elevated Expression of DNA Methyltransferases and Enhancer of Zeste Homolog 2 in Helicobacter pylori - Gastritis and Gastric Carcinoma. Dig Dis. 2022;40(2):156–67.

135. Ott HM, Graves AP, Pappalardi MB, Huddleston M, Halsey WS, Hughes AM, et al. A687V EZH2 is a driver of histone H3 lysine 27 (H3K27) hypertrimethylation. Mol Cancer Ther. 2014 Dec;13(12):3062–73.

136. Simon JA, Lange CA. Roles of the EZH2 histone methyltransferase in cancer epigenetics. Mutat Res. 2008 Dec 1;647(1–2):21–9.

137. Ying X, Pan R, Zhong J, Wu B, Jiang Y, Ying J, et al. Significant association of EED promoter hypomethylation with colorectal cancer. Oncol Lett. 2019 Aug;18(2):1564–70.

138. Zhang H, Feng Y, Si Y, Lu C, Wang J, Wang S, et al. Shank3 ameliorates neuronal injury after cerebral ischemia/reperfusion via inhibiting oxidative stress and inflammation. Redox Biol. 2024 Feb;69:102983.

139. Mitz AR, Boccuto L, Thurm A. Evidence for common mechanisms of pathology between SHANK3 and other genes of Phelan-McDermid syndrome. Clin Genet. 2024 May;105(5):459–69.

140. Phelan K, Rogers RC. Phelan-McDermid Syndrome. In: Adam MP, Ardinger HH, Pagon RA, Wallace SE, Bean LJ, Stephens K, et al., editors. GeneReviews®. Seattle (WA): University of Washington, Seattle; 1993.

141. De Falco D, Di Stasio D, Lauritano D, Lucchese A, Petruzzi M. Orofacial lymphedema in phelan–mcdermid syndrome: A case of hemifacial involvement and a scoping review. Appl Sci. 2025 Feb 19;15(4):2195.

142. Beri S, Tonna N, Menozzi G, Bonaglia MC, Sala C, Giorda R. DNA methylation regulates tissue-specific expression of Shank3. J Neurochem. 2007 Jun;101(5):1380–91.

143. Mu J, Slevin JC, Qu D, McCormick S, Adamson SL. In vivo quantification of embryonic and placental growth during gestation in mice using micro-ultrasound. Reprod Biol Endocrinol. 2008 Aug 12;6:34.

144. Rasband WS. ImageJ, U. S [Internet]. National Institutes of Health, Bethesda, Maryland, USA; 1997 [cited 2024 Feb 13]. Available from: https://imagej.net/ij/

145. Xie Q, Shen W-W, Zhong J, Huang C, Zhang L, Li J. Lipopolysaccharide/adenosine triphosphate induces IL-1β and IL-18 secretion through the NLRP3 inflammasome in RAW264.7 murine macrophage cells. Int J Mol Med. 2014 Jul;34(1):341–9.

146. Tighe RM, Birukova A, Yaeger MJ, Reece SW, Gowdy KM. Euthanasia- and Lavage-mediated Effects on Bronchoalveolar Measures of Lung Injury and Inflammation. Am J Respir Cell Mol Biol. 2018 Aug;59(2):257–66.

147. Al-Mousawi AM, Kulp GA, Branski LK, Kraft R, Mecott GA, Williams FN, et al. Impact of anesthesia, analgesia, and euthanasia technique on the inflammatory cytokine profile in a rodent model of severe burn injury. Shock. 2010 Sep;34(3):261–8.

148. Lawrance CC, Lucas EA, Clarke SL, Smith BJ, Kuvibidila S. Differential effects of isoflurane and CO2 inhalation on plasma levels of inflammatory markers associated with collagen-induced arthritis in DBA mice. Int Immunopharmacol. 2009 Jul;9(7–8):807–9.

149. Wilfinger WW, Mackey K, Chomczynski P. Effect of pH and ionic strength on the spectrophotometric assessment of nucleic acid purity. BioTechniques. 1997 Mar;22(3):474–6, 478.

150. Andersen CL, Jensen JL, Ørntoft TF. Normalization of real-time quantitative reverse transcription-PCR data: a model-based variance estimation approach to identify genes suited for normalization, applied to bladder and colon cancer data sets. Cancer Res. 2004 Aug 1;64(15):5245–50.

151. Pfaffl MW. A new mathematical model for relative quantification in real-time RT-PCR. Nucleic Acids Res. 2001 May 1;29(9):e45.

152. Ward EJ, Bert S, Fanti S, Malone KM, Maughan RT, Gkantsinikoudi C, et al. Placental inflammation leads to abnormal embryonic heart development. Circulation. 2023 Mar 21;147(12):956–72.

153. Ashland OR. FlowJo™ Software. Becton, Dickinson and Company; 2023.

154. Krueger F, Andrews SR. Bismark: a flexible aligner and methylation caller for Bisulfite-Seq applications. Bioinformatics. 2011 Jun 1;27(11):1571–2.

155. Akalin A, Kormaksson M, Li S, Garrett-Bakelman FE, Figueroa ME, Melnick A, et al. methylKit: a comprehensive R package for the analysis of genome-wide DNA methylation profiles. Genome Biol. 2012 Oct 3;13(10):R87.

156. Wang J, Vasaikar S, Shi Z, Greer M, Zhang B. WebGestalt 2017: a more comprehensive, powerful, flexible and interactive gene set enrichment analysis toolkit. Nucleic Acids Res. 2017 Jul 3;45(W1):W130–7.

157. Li L-C, Dahiya R. MethPrimer: designing primers for methylation PCRs. Bioinformatics. 2002 Nov;18(11):1427–31.

158. Gene Codes Corp. Sequencher®. Ann Arbor, MI, USA: 1991; 2023.

Fig. 2. Maternal pro-inflammatory activation induces embryonic axial differences in cytokine and *Cdh1* expression

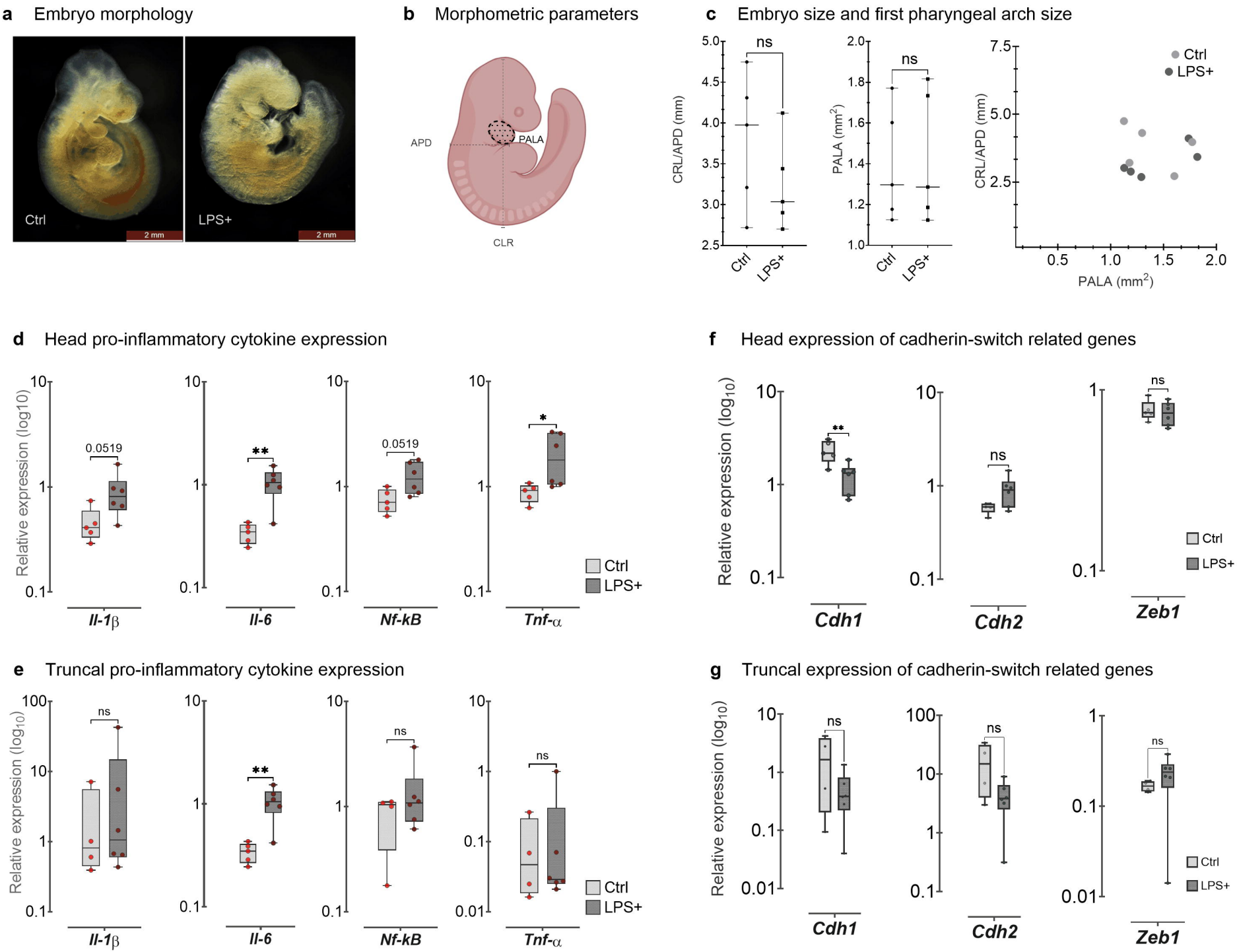

Fig. 3. Pro-inflammatory response in the embryo head epigenetically downregulates neural crest *Cdh1*/E-cadherin

a Levels of E-cadherin protein in neural crest cells

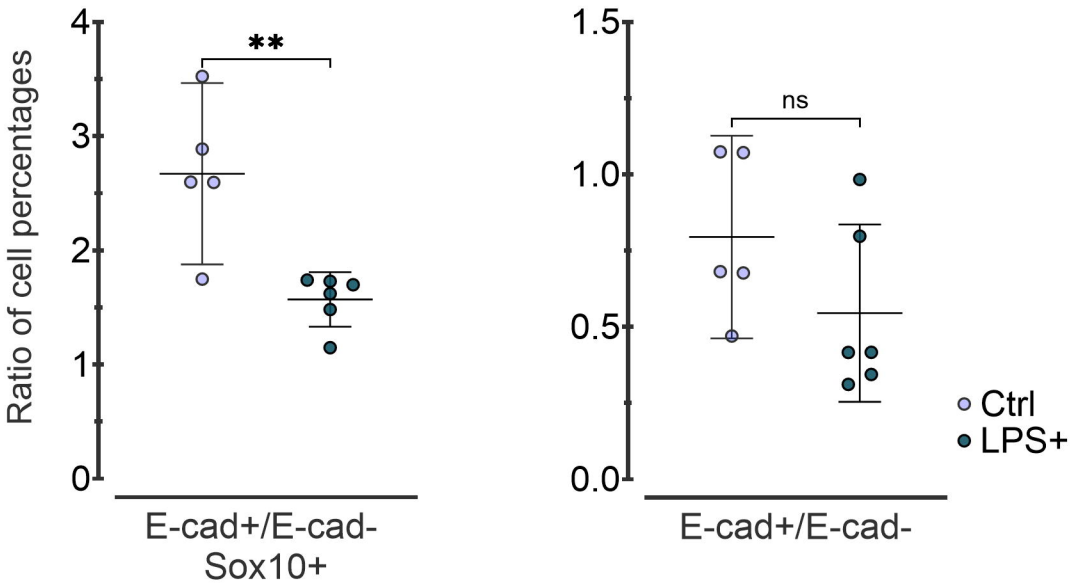

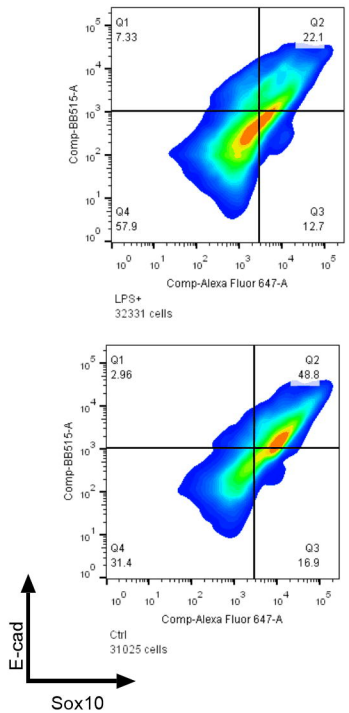

b Cdh1 promoter methylation

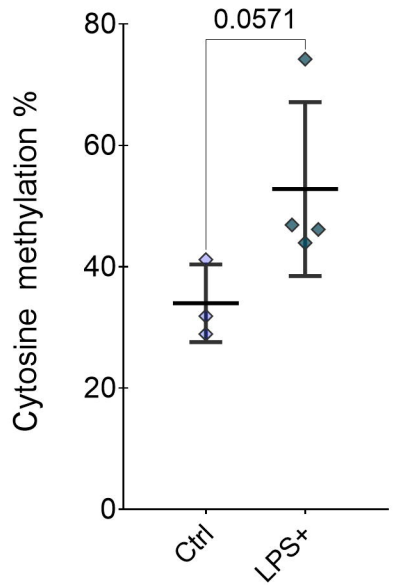

c Expression of neuroepithelium markers

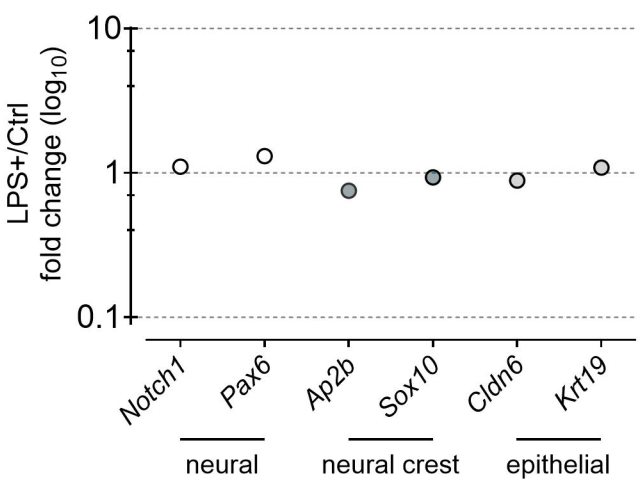

d Expression of methyltransferases

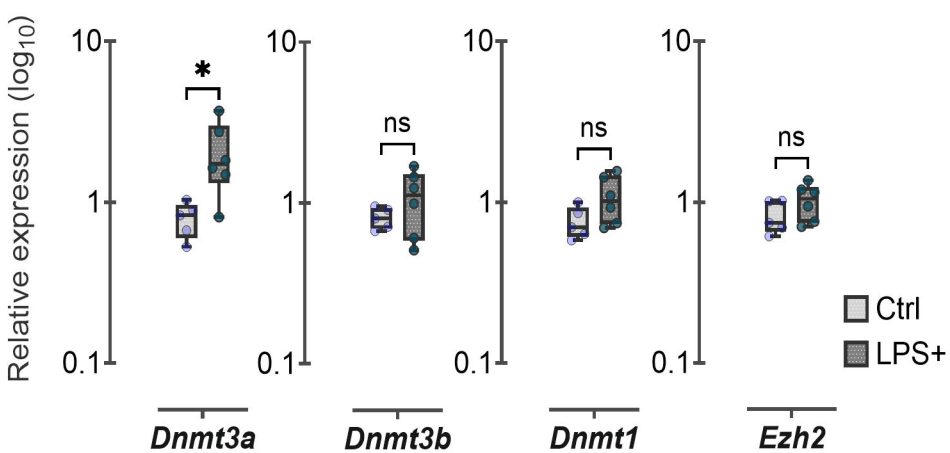

e Nuclear DNMT activity

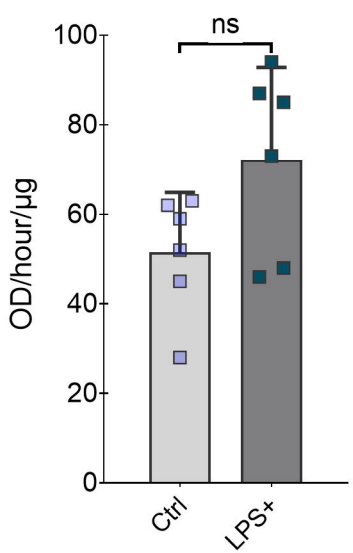

Fig. 4. *Cdh1* single dose silencing in combination with pro-inflammatory insult drives craniofacial and neural tube malformations

a Craniofacial and neural tube alterations induced by LPS

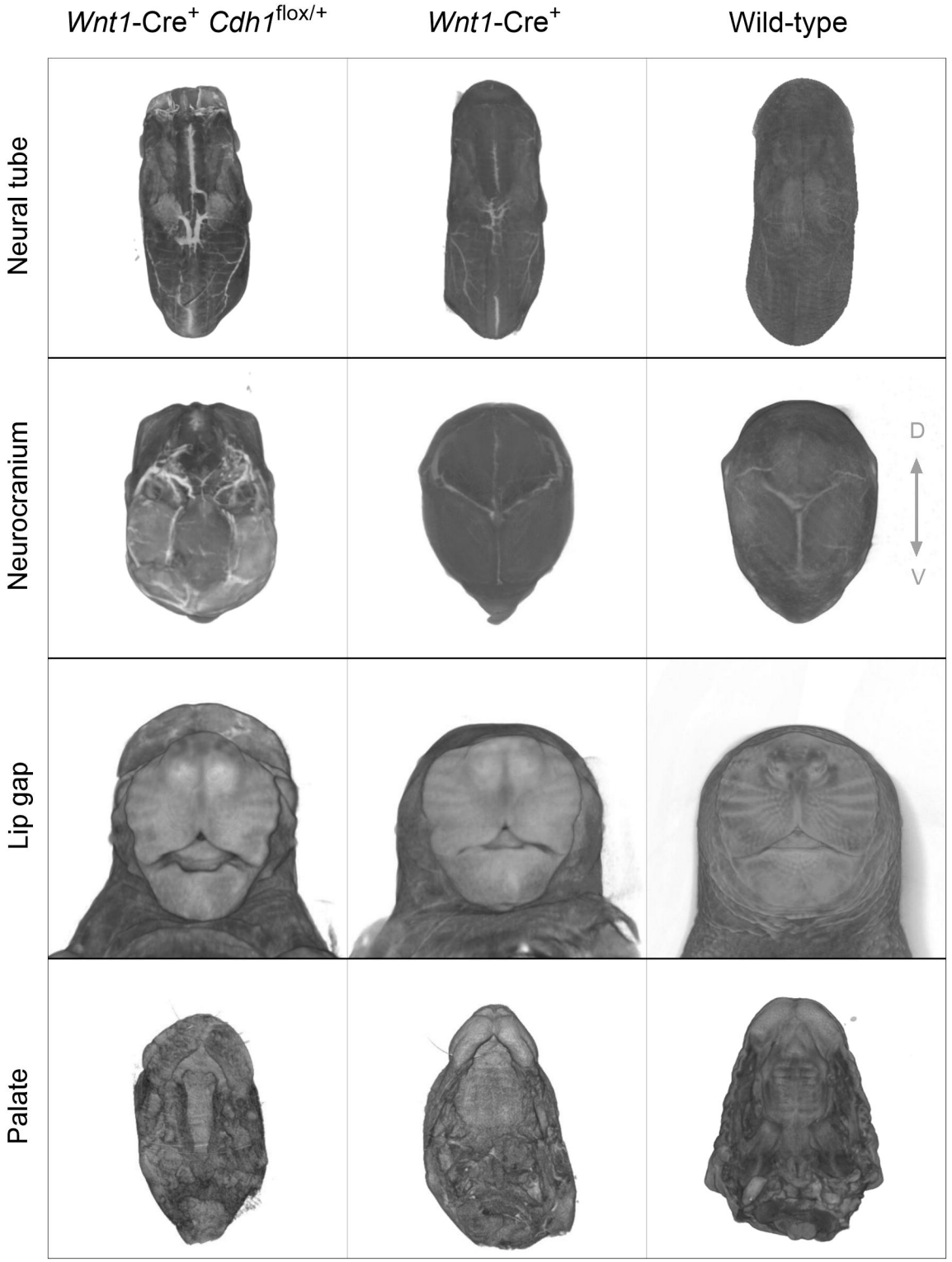

b Lip gap size

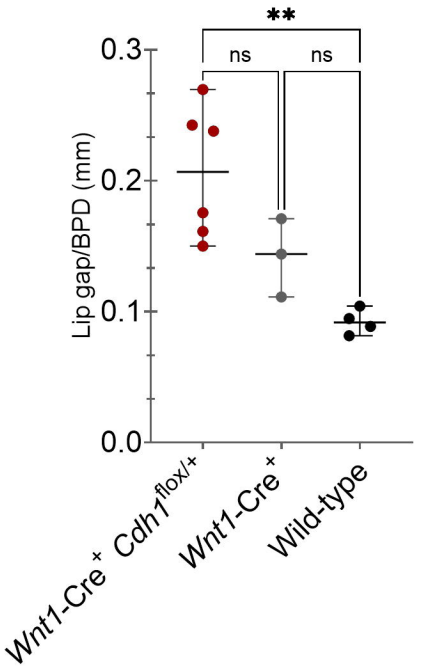

c Embryo size

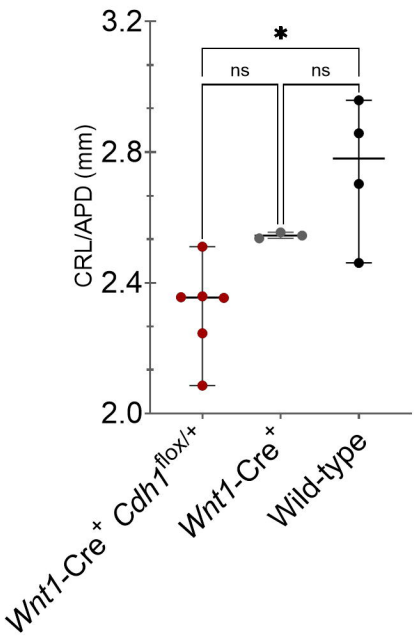
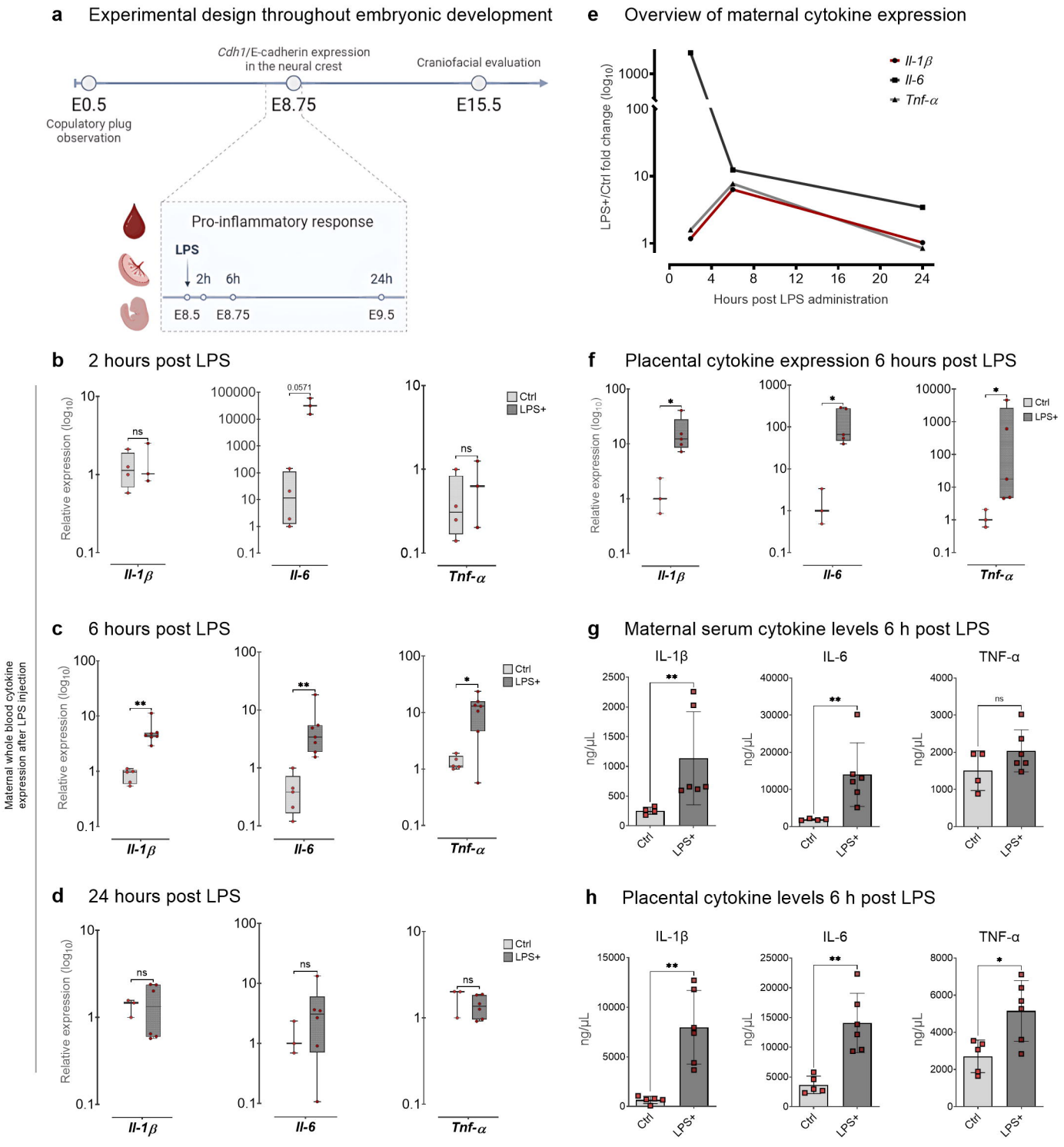
Fig. 1. LPS activates systemic and placental pro-inflammatory cytokine expression